ELSEVIER

Chemical Geology 234 (2006) 264–290

CHEMICAL GEOLOGY
INCLUDING ISOTOPE GEOSCIENCE

www.elsevier.com/locate/chemgeo

# Magma chamber processes in the Tellnes ilmenite deposit (Rogaland Anorthosite Province, SW Norway) and the formation of Fe–Ti ores in massif-type anorthosites

B. Charlier *, J.-C. Duchesne, J. Vander Auwera

*Department of Geology, B20, University of Liège, B-4000 Sart Tilman, Belgium*

Received 29 September 2005; received in revised form 5 May 2006; accepted 12 May 2006

**Abstract**

The origin of igneous Fe–Ti oxide ores associated with massif-type anorthosites is investigated through a detailed study of the world-class Tellnes ilmenite deposit, part of the late-Proterozoic (930–920 Ma) AMC series of the Rogaland Anorthosite Province (SW Norway). More than 100 samples from drill cores reveal significant petrographical and compositional variations within the ore body. Four zones are defined, based on variations in modal proportions and cumulus mineral assemblages: the Lower and Upper Central Zones and the Lower and Upper Marginal Zones. Plagioclase and whole-rock compositions discriminate the zones and display patterns interpreted as a result of mixing of either plagioclase–ilmenite or plagioclase–ilmenite–orthopyroxene–olivine cumulates with a melt of ferrodioritic (jotunitic) composition with a content decreasing from 80 to 20% from the margins to the central part of the ore body. Phase diagrams for a jotunitic parental magma reproduce the crystallization sequence at 5 kb. The orthopyroxene–olivine liquidus boundary is a peritectic in the Bjerkreim-Sokndal layered intrusion and a cotectic in Tellnes and this explains the differences in the sequence of crystallization of the two intrusions. The high concentration of ilmenite, well above cotectic proportions, resulted from gravity-sorting in the Tellnes ore body, which represents the lower part of a larger magma chamber. Uniform Sr isotope ratios do not support magma mixing. The cryptic layering of the ore body precludes injection as a crystal mush but favours in situ crystallization from an evolving magma in a sill-like magma chamber. The present trough-shape and mineral orientations result from deformation during gravity-induced subsidence and by up-doming of the anorthosite. Fractional crystallization of a $TiO_2$-rich magma with ilmenite as an early liquidus mineral and plagioclase buoyancy are the principal mechanisms responsible for the formation of Fe–Ti deposits in Proterozoic massif-type anorthosites.


*Keywords:* Anorthosite; Fe–Ti deposits; Tellnes; Magma chamber processes; Cumulate; Trapped liquid

## 1. Introduction

Economic igneous Fe–Ti oxide occurrences are commonly associated with massif-type anorthosites and two hard-rock deposits are currently being mined: the Tellnes ilmenite deposit (Rogaland Anorthosite Province, SW Norway) and the Lac Tio deposit (Allard Lake anorthosite, Quebec, Canada). The scarcity of Fe–Ti deposits has hampered research on the formation of such ore bodies and particularly on mechanisms responsible for ilmenite enrichment. There is no consensus as to whether accumulation processes, immiscibility, magma mixing, fractional crystallization, solid-state remobilisation, cotectic

* Corresponding author. Tel.: +32 4 3662250; fax: +32 4 3662921.
*E-mail address:* b.charlier@ulg.ac.be (B. Charlier).

0009-2541/$ - see front matter © 2006 Elsevier B.V. All rights reserved.
doi:10.1016/j.chemgeo.2006.05.007

crystallization, or a combination of these processes or others, control the formation of Fe–Ti oxide ores. Nevertheless, the genesis of massif-type anorthosites and related rocks has been thoroughly debated (e.g. Ashwal, 1993; Longhi et al., 1999; Vander Auwera et al., 2000; Bédard, 2001; Longhi, 2005) and the Rogaland Anorthosite Province in particular has been the subject of numerous investigations (see Duchesne, 2001 for a review). In this province, the Bjerkreim-Sokndal layered intrusion, which contains all rock types belonging to the AMC series (Anorthosite–Mangerite–Charnockite), has been extensively studied (see Wilson et al., 1996 for a review). The petrogenesis of the Bjerkreim-Sokndal Intrusion has greatly improved our understanding of the origin of massif-type anorthosites and related rocks. An important feature of the AMC series in Rogaland is the inferred jotunitic (hypersthene monzodiorite) parental magma. These liquids, also called ferrodiorites (Ashwal, 1993; Emslie et al., 1994), are Fe-, Ti- and P-rich and, contrary to basaltic magmas, crystallize ilmenite as an early liquidus mineral. The liquid line of descent of jotunitic magma is well known due to the occurrence of fine-grained jotunitic dykes that represent liquid compositions (Duchesne et al., 1989) and as a result of experimental studies (Vander Auwera et al., 1998) performed on such compositions.

In this well-documented geological context, a comprehensive genetic model for the Tellnes ilmenite deposit remains to be established. This deposit, which has been mined since 1960 by TITANIA A/S, was previously described as a rather homogeneous ore body with plagioclase, ilmenite, and orthopyroxene as the major minerals (Gierth and Krause, 1973). However, an extensive database of whole-rock compositions built up by TITANIA A/S over the last twenty years indicates that compositional variations are larger than previously believed. A detailed petrographical and geochemical investigation of more than 100 samples from the deposit has thus been undertaken in order to constrain a genetic model for the ore body and Fe–Ti ore-forming processes in massif-type anorthosites in general.

## 2. Geological setting

### 2.1. The Rogaland Anorthosite Province

The Tellnes ilmenite deposit belongs to the late-Proterozoic Rogaland Anorthosite Province (see Duchesne, 2001 for a review), emplaced in the south-western part of the Sveconorwegian orogenic belt (SW Norway) (Fig. 1). The Province comprises different units of the AMC series: four large massif-type anorthosite plutons (Egersund-Ogna, Håland, Helleren and Åna-Sira), the Bjerkreim-Sokndal layered intrusion (Wilson et al., 1996), two smaller leuconoritic bodies (Hidra and Garsaknatt) (Demaiffe, 1977; Demaiffe and Hertogen, 1981), minor intrusions (Vander Auwera et al., in press) and dykes of the jotunitic (hypersthene monzodiorite) kindred (Duchesne et al., 1989). Another characteristic is the presence of numerous Fe–Ti deposits of subeconomic to economic grade (e.g. Tellnes), occurring in the Åna-Sira, Håland and Helleren anorthosites (Duchesne, 1999).

These magmatic rocks were emplaced between 930 and 920 Ma (Schärer et al., 1996) in granulite facies ortho- and paragneisses, generating a wide, high-temperature contact metamorphic aureole (Maijer, 1987; Möller et al., 2002). Intrusion of the Rogaland Anorthosite Province took place some 40 Ma after the Sveconorwegian orogeny (Bingen and van Breemen, 1998; Bingen and Stein, 2003) in a post-collisional regime (Duchesne et al., 1999). No subsequent metamorphism has overprinted this magmatic event. The anorthosite plutons crystallized over a large range of pressures, starting at about 11 to 13 kb in large magma chambers in the lower part of a thickened crust (Longhi et al., 1993, 1999; Longhi, 2005). The low density of a plagioclase crystal mush induced diapiric uprise of the anorthositic massifs, possibly through zones of weakness (Scoates and Chamberlain, 1997), to their final intrusion at a pressure of around 5 kb (Ashwal, 1993; Duchesne et al., 1999). Deformation observed in the Province can be accounted for by anorthosite emplacement (Barnichon et al., 1999) and gravity instabilities (Bolle et al., 2002). Late doleritic dykes cross-cut the Province and are related to the opening of the Iapetus Ocean at 616±3 Ma (Bingen et al., 1998).

### 2.2. The Tellnes ilmenite ore body

The ore body, an ilmenite-rich norite averaging slightly more than 18% $TiO_2$, was discovered in 1954 during an aeromagnetic survey, and production started 6 years later by TITANIA A/S as an open-pit mine. Reserves are estimated to be 57 Mt $TiO_2$, representing 14% of the world reserves of ilmenite and 12% of the total (ilmenite+rutile) world reserves of titanium minerals. By-products are magnetite and Ni–Cu sulphide concentrates.

The Tellnes ore body is intruded into the central part of the Åna-Sira anorthosite (Gierth and Krause, 1973; Krause et al., 1985) (Fig. 1). This anorthosite body is essentially made up of granulated plagioclase with rare isolated Al-rich orthopyroxene megacrysts. Some parts are leuconoritic, containing plagioclase, orthopyroxene and ilmenite. The massif contains numerous Fe–Ti deposits which have been mined in the past. The most important of these occurrences are Storgangen, Bøstølen, and Blåfjell (Fig. 1) (Krause and

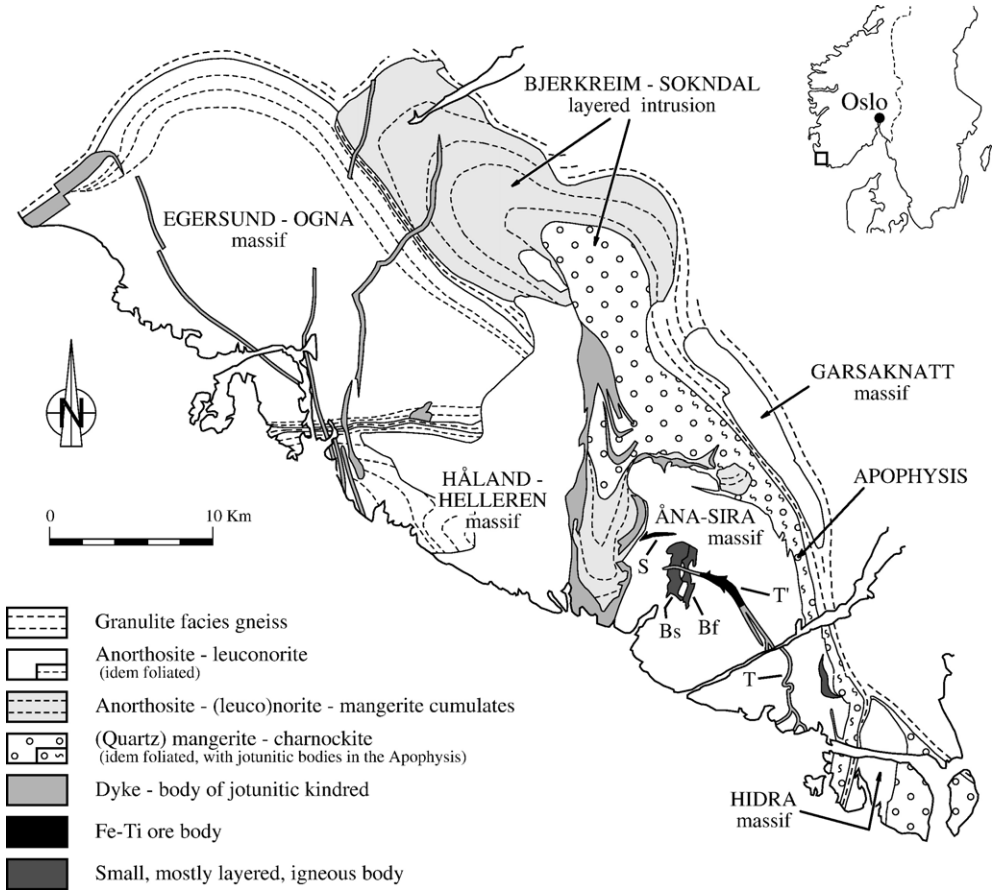


Fig. 1. Geological map of the Rogaland Anorthosite Province (after Bolle, 1996) showing the location of the Tellnes ilmenite deposit in the central part of the Åna-Sira anorthosite. Bs: Bøstølen intrusion; Bf: Blåfjell deposit; S: Storgangen; T: Tellnes "main dyke"; T': Tellnes ilmenite deposit. Late doleritic dykes are not shown.

Zeino-Mahmalat, 1970; Krause and Pape, 1977; Krause et al., 1985; Duchesne, 1999). Mining is now confined to Tellnes (Fig. 2). This deposit crosscuts the anorthosite and thus seems to be younger than its host; U–Pb ages of zircon is 920±3 Ma for the ore body and 932±3 Ma for the anorthosite (Schärer et al., 1996). However, Charlier et al. (submitted for publication) have concluded that the 920 Ma age for Tellnes reflects the timing of Zr exsolution from ilmenite and not the age of crystallization, which is probably closer to the age of the anorthosite of around 930 Ma.

The deposit has a sickle-shape oriented WNW–ESE to NNW–SSE and has a maximum width and length of 400 m and 2700 m respectively. The intrusive character of the ore body is demonstrated by sharp contacts with the host anorthosite, numerous apophyses and anorthosite xenoliths, particularly abundant in the south-eastern part. The main body extends to the NW and SE as a dyke (the "main dyke") with a jotunitic to charnockitic composition (Wilmart et al., 1989). Dated at 931±5 Ma (U–Pb ages on zircon; Schärer et al., 1996), the dyke is not comagmatic with the ore deposit, as shown by different Sr isotope ratios (Wilmart et al., 1989). The two intrusions were successively emplaced in the same structure, produced by a transcurrent, dextral opening of a WNW–ESE-striking zone of weakness in the Åna-Sira anorthosite (Diot et al., 2003). Two sub-vertical doleritic dykes oriented WNW–ESE cut the Tellnes deposit.

## 3. Previous studies

Detailed petrographical descriptions of the Tellnes ilmenite deposit have been presented by Gierth (1970), Gierth and Krause (1973, 1974), Gierth et al. (1982) and Gierth (1983). Although these authors describe the mineralogical and chemical composition of the ore body as very uniform, they noticed some variability. Most important are the lower ilmenite and the higher

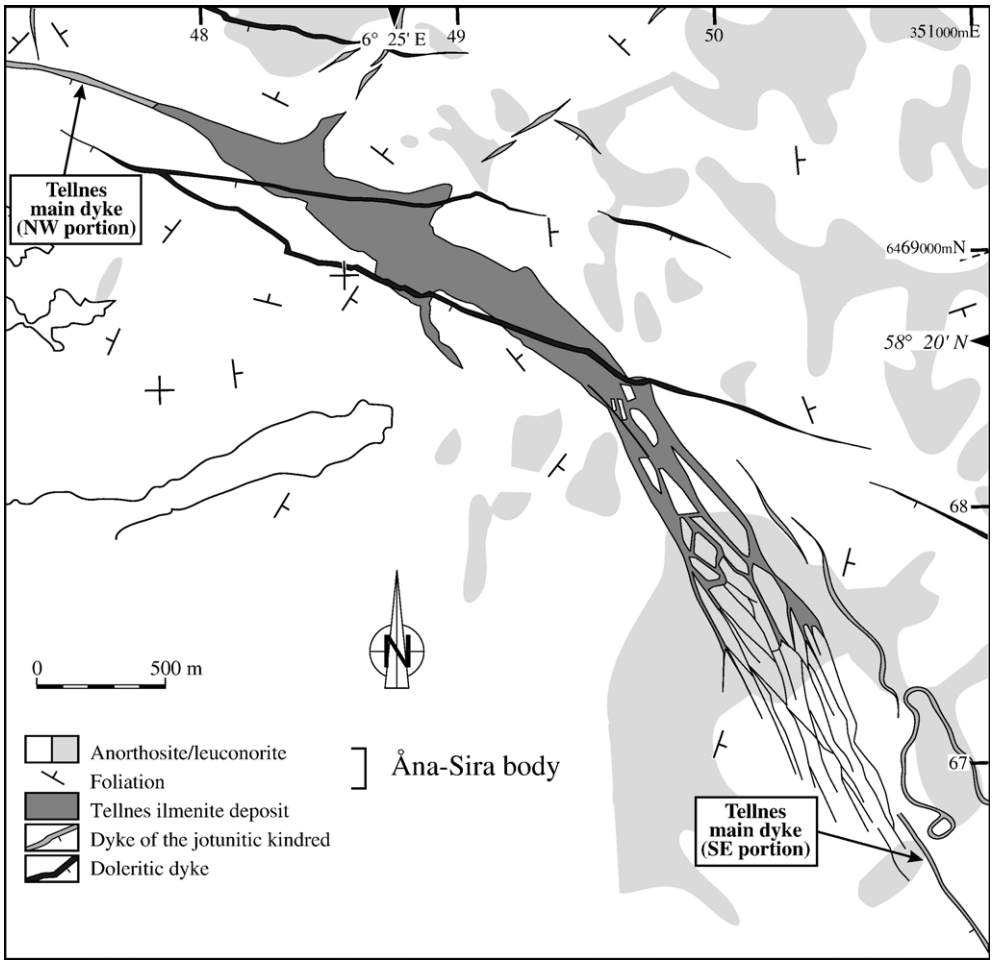


Fig. 2. Geological map of the Tellnes ilmenite deposit and the host Åna-Sira anorthosite at present level of exposure (after Krause et al., 1985). Grid is the EURF89 kilometric UTM. Minor late faults are not shown.

plagioclase and apatite contents at the margins of the ore body. The upper part contains increasing amounts of magnetite and sulphides whereas the lower part is almost magnetite-free and poor in sulphides.

Wilmart et al. (1989) reported a detailed geochemical study (Sr isotopes, major and trace elements) of the Tellnes dyke and the ore body. They inferred that the ilmenite-rich norite could have been derived by crystallization of a noritic liquid related to the host Åna-Sira anorthosite. An emplacement mechanism involving injection of a noritic crystal-mush, lubricated by 3 to 10% trapped liquid, was proposed by Wilmart et al. (1989). In this model, the ilmenite enrichment was explained by dynamic sorting of dense ilmenite during movement of the mush and its progressive accumulation to form the ilmenite-rich norite in the more central part of the conduit. The less dense plagioclase-rich part of the mush was emplaced at the margins and in the SE apophyses of the ore body. Emplacement as a crystal-mush was later supported by magnetic and petrofabric evidence (Diot et al., 2003). The shape orientation of minerals was interpreted to have resulted from flow during injection of the ilmenite norite mush. From the well-constrained plunge of the lineation (averaging SE 18°), Diot et al. (2003) concluded that the mush was derived from an adjacent (unexposed) magma chamber and was injected laterally and slightly upwards from the SE into a zone of weakness.

Robinson et al. (2003) recently compared the Tellnes deposit to ilmenite-rich cumulates of the Bjerkreim-Sokndal layered intrusion. In the latter, magma mixing is inferred and the hybrid magma appears to have crystallized relatively large amounts of ilmenite (Wilson

et al., 1996). Comparable compositional ranges of plagioclase and orthopyroxene in Tellnes and in Bjerkreim-Sokndal have led Robinson et al. (2003) to suggest a similar origin for the two types of cumulates: comparable parental magmas and possibly similar mixing events but within chambers of different shapes. Nevertheless, these authors admit that further documentation based on more detailed mineralogical and petrological studies is needed.

Extensive drilling by the mining company and microgravimetric analyses have resulted in a detailed picture of the 3D-shape of the ore body (Fig. 3). A huge database of whole-rock compositions has also been compiled by TITANIA A/S (Kullerud, 2003). About 5000 samples have been analysed for $TiO_2$, $P_2O_5$, Cr, S and modal magnetite. Of these, 2000 samples have been analysed for all major elements and selected trace elements. Based on compositional variations within the ore body, Kullerud (2003) recognized four zones: a Lower Central Zone (LCZ: ilmenite-rich, plagioclase- and Fe–Mg silicate-poor), an Upper Central Zone (UCZ: ilmenite- and Fe–Mg silicate-rich, plagioclase-poor), a Lower Marginal Zone (LMZ: plagioclase-rich, ilmenite- and Fe–Mg silicate-poor), and an Upper Marginal Zone (UMZ: plagioclase- and Fe–Mg silicate-rich, ilmenite-poor). These observations have, however, not resulted in a new interpretation of the origin of the ore body.

## 4. Samples and analytical methods

More than 100 samples were selected from various drill cores in three SSW–NNE sections (800, 1200 and 1600), more or less perpendicular to the elongation of the ore body (Fig. 4). Each sample corresponds to 40 cm to 1 m of a split drill core. Altered portions of rocks have been avoided during sampling. A few rocks were also collected in the open-pit. Petrographic studies were carried out on polished thin sections for all rocks.

Forty seven samples were selected from sections 800, 1200 and 1600 for plagioclase separation (Fig. 4). Mineralogical separation of plagioclase grains (60–150 μm) was performed using flotation in bromoform and a Frantz isodynamic magnetic separator. Final purification was carried out by HCl leaching to dissolve any apatite grains and by hand-picking under the microscope. Samples were ground in an agate mortar and analysed for major elements by XRF on Li-borate fused glass and for Sr and Ba by XRF on pressed powder pellets (Table 1).

Sr isotopic ratios were measured for twenty one of these plagioclase samples on a Fisons VG Sector 54 mass spectrometer using dynamic multicollection at the Université Libre de Bruxelles (Table 2). Prior to separation using ion exchange resin, plagioclase separates were

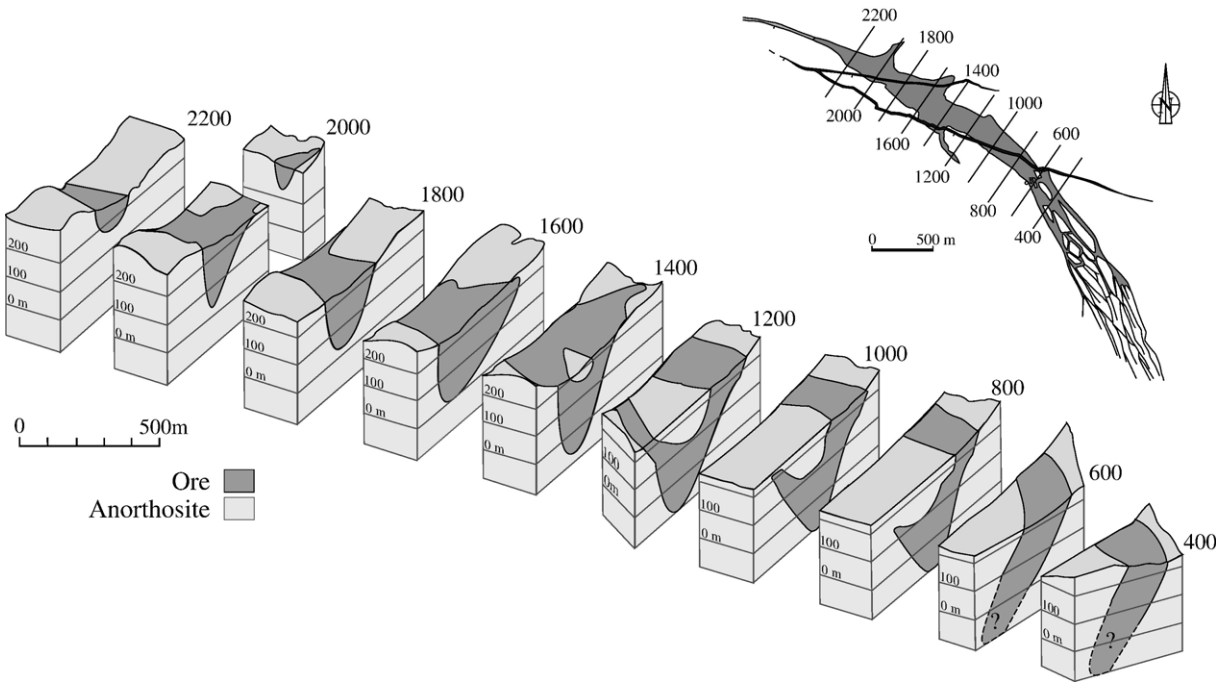


Fig. 3. 3D view of the Tellnes ilmenite deposit constructed from drill cores and microgravimetric data with level of exposure before mining activity (modified after Diot et al., 2003). Doleritic dykes not shown in 3D.

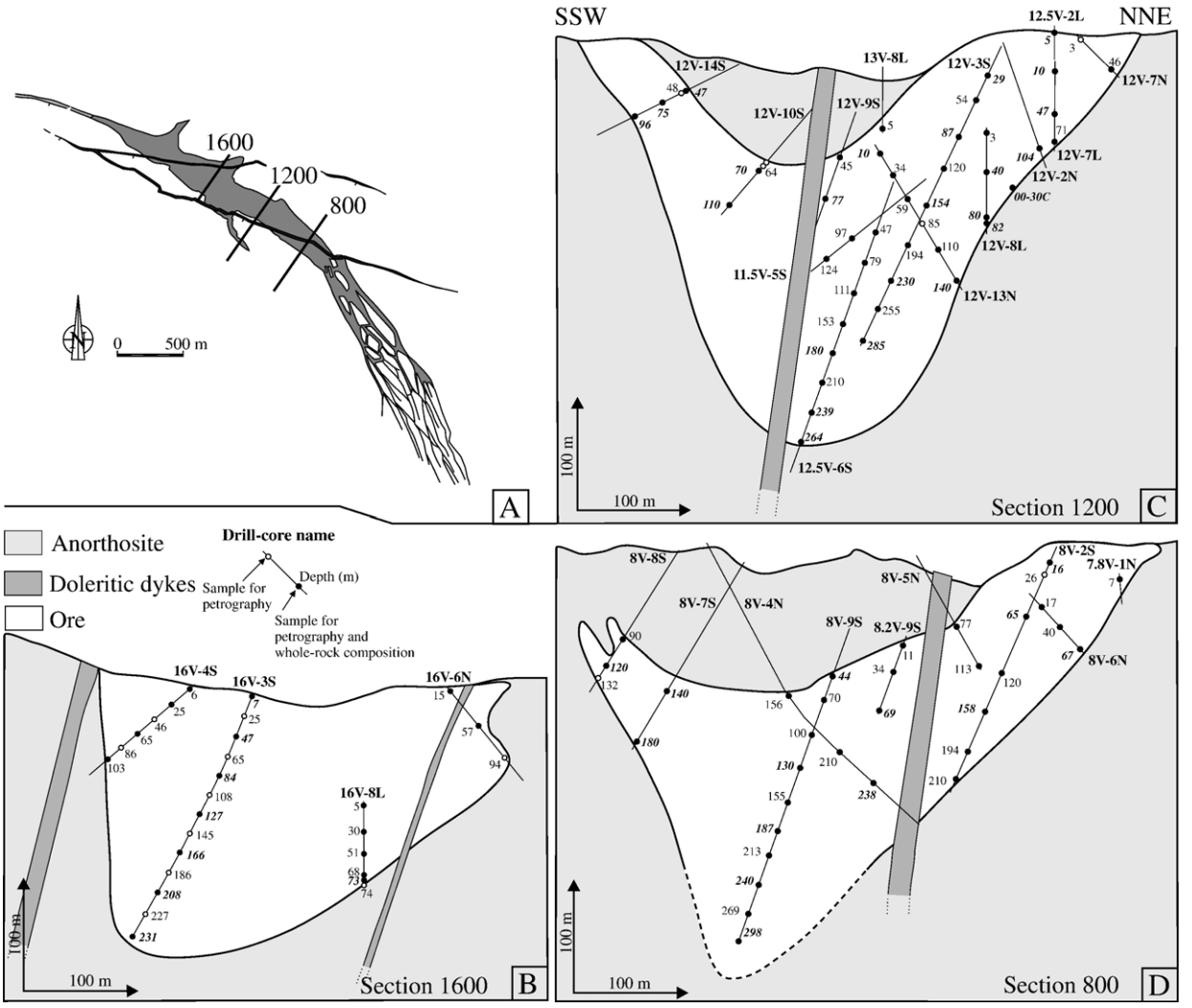


Fig. 4. (A) Location of the three selected cross sections on the geological map of the Tellnes ilmenite deposit (same legend as Fig. 2); (B–D) Spatial distribution of selected drill holes and samples in cross sections 1600, 1200 and 800. Bold numbers in italics are samples from which plagioclase has been separated. The dotted bottom of the intrusion in section 800 has not been intersected by drill cores but is interpreted.

dissolved in a mixture of HF, $HNO_3$ and $HClO_4$. During the period of measurements, $^{87}Sr/^{86}Sr$ for the NBS897 Sr standard was 0.710273±0.000007 (normalized to $^{86}Sr/^{88}Sr$=0.1194).

Whole-rock compositions for 97 samples were analysed for major elements by XRF on Li-borate fused glass (Table 3). All the XRF analyses were performed on the ARL 9400 XP at the University of Liege (Belgium). Accuracy and reproducibility were evaluated on the basis of a collection of international standards (Bologne and Duchesne, 1991). Modal proportions have been determined by point counting (2000 points per 3×4.5 cm thin section). Modal proportions are expressed as wt.%, converted from the volume% using appropriate mineral densities (Table 3).

## 5. Petrography

### 5.1. Mineralogy and textural relationships

The Tellnes ore is an equigranular, massive, medium-grained (~0.5–2 mm) ilmenite-rich norite. The norite rarely displays modal layering and appears extremely homogeneous in outcrop. Plagioclase, ilmenite and orthopyroxene are the main minerals. Olivine, magnetite, clinopyroxene, biotite, apatite and hornblende are subordinate. Traces of Fe–Ni–Co–Cu sulphides are ubiquitous. Other accessory phases include aluminous spinel, baddeleyite and zircon.

Plagioclase is the most abundant mineral in the ore. It forms elongated laths ranging from 0.5 to 2 mm in

Table 1
Composition of plagioclase separates (XRF analyses) from the Tellnes ilmenite deposit

| Sample | Depth | Zone | $SiO_2$ | $TiO_2$ | $Al_2O_3$ | $Fe_2O_3$ | MgO | CaO | $Na_2O$ | $K_2O$ | $P_2O_5$ | Total | An[a] | Or[b] | Sr | Ba |
|---|---|---|---|---|---|---|---|---|---|---|---|---|---|---|---|---|
| P8V-4N | 238 | UCZ | 57.26 | 0.10 | 26.96 | 0.19 | 0.14 | 9.51 | 5.73 | 0.54 | 0.01 | 100.45 | 47.8 | 3.1 | 1170 | 169 |
| P8V-6N | 67 | UMZ | 58.53 | 0.05 | 26.15 | 0.21 | 0.13 | 8.62 | 6.11 | 0.72 | 0.01 | 100.54 | 43.8 | 4.2 | 1103 | 231 |
| P8V-2S | 16 | UCZ | 58.27 | 0.08 | 26.19 | 0.18 | 0.08 | 8.65 | 6.29 | 0.53 | 0.01 | 100.29 | 43.2 | 3.1 | 1162 | 212 |
| P8V-2S | 65 | UCZ | 58.52 | 0.07 | 26.35 | 0.20 | 0.08 | 8.72 | 5.88 | 1.01 | 0.01 | 100.85 | 45.0 | 5.8 | 1051 | 284 |
| P8V-2S | 158 | UCZ | 57.75 | 0.09 | 26.64 | 0.21 | 0.25 | 9.12 | 5.96 | 0.54 | 0.01 | 100.58 | 45.8 | 3.1 | 1147 | 168 |
| P8V-7S | 140 | LMZ | 57.98 | 0.09 | 26.75 | 0.21 | 0.08 | 9.22 | 5.91 | 0.58 | 0.01 | 100.84 | 46.3 | 3.4 | 1143 | 195 |
| P8V-7S | 180 | LCZ | 57.81 | 0.04 | 26.67 | 0.20 | 0.22 | 9.20 | 5.96 | 0.53 | 0.01 | 100.65 | 46.0 | 3.1 | 1156 | 180 |
| P8V-8S | 120 | LMZ | 58.70 | 0.04 | 26.39 | 0.20 | 0.09 | 8.73 | 6.14 | 0.62 | 0.01 | 100.93 | 44.0 | 3.6 | 1153 | 204 |
| P8V-9S | 44 | UCZ | 57.96 | 0.06 | 26.43 | 0.28 | 0.35 | 8.96 | 5.92 | 0.74 | 0.01 | 100.72 | 45.5 | 4.3 | 1098 | 225 |
| P8V-9S | 130 | UCZ | 57.32 | 0.06 | 27.04 | 0.20 | 0.11 | 9.55 | 5.74 | 0.54 | 0.01 | 100.58 | 47.9 | 3.1 | 1170 | 186 |
| P8V-9S | 187 | LCZ | 57.32 | 0.04 | 27.08 | 0.23 | 0.21 | 9.64 | 5.59 | 0.64 | 0.01 | 100.77 | 48.8 | 3.7 | 1155 | 206 |
| P8V-9S | 240 | LCZ | 56.96 | 0.05 | 26.91 | 0.28 | 0.56 | 9.54 | 5.54 | 0.58 | 0.01 | 100.44 | 48.8 | 3.4 | 1163 | 187 |
| P8V-9S | 298 | LCZ | 57.50 | 0.04 | 26.88 | 0.22 | 0.38 | 9.48 | 5.67 | 0.55 | 0.01 | 100.74 | 48.0 | 3.2 | 1152 | 180 |
| P8.2V-9S | 69 | UCZ | 57.15 | 0.06 | 26.77 | 0.25 | 0.24 | 9.39 | 5.73 | 0.55 | 0.01 | 100.16 | 47.5 | 3.2 | 1151 | 179 |
| P12V-2N | 104 | UMZ | 58.40 | 0.04 | 26.03 | 0.26 | 0.16 | 8.60 | 6.03 | 0.86 | 0.01 | 100.40 | 44.1 | 5.0 | 1068 | 252 |
| P12V-13N | 10 | UCZ | 56.41 | 0.06 | 27.00 | 0.28 | 0.15 | 9.34 | 6.03 | 0.59 | 0.02 | 99.88 | 46.1 | 3.4 | 1153 | 181 |
| P12V-13N | 140 | LMZ | 58.06 | 0.04 | 26.49 | 0.21 | 0.07 | 9.02 | 5.89 | 0.73 | 0.01 | 100.53 | 45.8 | 4.2 | 1118 | 206 |
| P12V-3S | 29 | UCZ | 56.40 | 0.06 | 26.75 | 0.20 | 0.14 | 9.23 | 6.06 | 0.63 | 0.02 | 99.49 | 45.7 | 3.6 | 1142 | 187 |
| P12V-3S | 87 | UCZ | 55.88 | 0.06 | 27.09 | 0.23 | 0.11 | 9.55 | 5.88 | 0.53 | 0.02 | 99.35 | 47.3 | 3.0 | 1144 | 158 |
| P12V-3S | 154 | UCZ | 56.28 | 0.06 | 26.98 | 0.21 | 0.11 | 9.45 | 6.00 | 0.54 | 0.02 | 99.65 | 46.5 | 3.1 | 1153 | 162 |
| P12V-3S | 230 | LCZ | 56.08 | 0.05 | 27.14 | 0.19 | 0.08 | 9.65 | 5.98 | 0.51 | 0.02 | 99.70 | 47.1 | 2.9 | 1182 | 161 |
| P12V-3S | 285 | LCZ | 56.00 | 0.04 | 27.01 | 0.24 | 0.06 | 9.63 | 5.83 | 0.64 | 0.02 | 99.47 | 47.7 | 3.6 | 1162 | 199 |
| P12V-9S | 77 | UCZ | 57.20 | 0.06 | 26.91 | 0.28 | 0.20 | 9.48 | 5.68 | 0.57 | 0.01 | 100.40 | 48.0 | 3.3 | 1166 | 191 |
| P12V-10S | 70 | UCZ | 56.07 | 0.06 | 26.83 | 0.22 | 0.10 | 9.29 | 6.02 | 0.57 | 0.02 | 99.18 | 46.0 | 3.3 | 1166 | 184 |
| P12V-10S | 110 | LCZ | 57.35 | 0.05 | 26.88 | 0.26 | 0.29 | 9.34 | 5.73 | 0.61 | 0.01 | 100.53 | 47.4 | 3.6 | 1150 | 185 |
| P12V-14S | 47 | LMZ | 58.92 | 0.03 | 25.84 | 0.24 | 0.21 | 8.25 | 6.12 | 0.88 | 0.01 | 100.51 | 42.7 | 5.1 | 1048 | 271 |
| P12V-14S | 75 | LCZ | 56.91 | 0.05 | 26.70 | 0.21 | 0.14 | 9.04 | 6.34 | 0.50 | 0.02 | 99.91 | 44.1 | 2.8 | 1133 | 154 |
| P12V-14S | 96 | LMZ | 57.22 | 0.04 | 26.29 | 0.27 | 0.20 | 8.63 | 6.27 | 0.81 | 0.02 | 99.75 | 43.2 | 4.6 | 1092 | 244 |
| P12V-7L | 10 | UCZ | 57.40 | 0.06 | 26.90 | 0.31 | 0.27 | 9.38 | 5.78 | 0.53 | 0.02 | 100.66 | 47.3 | 3.1 | 1148 | 170 |
| P12V-7L | 47 | UCZ | 58.23 | 0.05 | 26.44 | 0.26 | 0.15 | 8.92 | 6.09 | 0.63 | 0.01 | 100.79 | 44.7 | 3.6 | 1123 | 192 |
| P12V-8L | 40 | UCZ | 57.80 | 0.06 | 26.80 | 0.21 | 0.11 | 9.26 | 5.93 | 0.52 | 0.01 | 100.71 | 46.3 | 3.0 | 1165 | 178 |
| P12V-8L | 80 | UMZ | 56.59 | 0.04 | 26.87 | 0.22 | 0.09 | 9.28 | 6.03 | 0.70 | 0.02 | 99.84 | 46.0 | 4.0 | 1130 | 205 |
| P12V-8L | 82 | UMZ | 57.24 | 0.04 | 26.06 | 0.22 | 0.10 | 8.41 | 6.23 | 0.99 | 0.02 | 99.31 | 42.7 | 5.6 | 1051 | 278 |
| P12.5V-6S | 180 | LCZ | 56.09 | 0.04 | 27.15 | 0.23 | 0.11 | 9.69 | 5.87 | 0.58 | 0.01 | 99.77 | 47.7 | 3.3 | 1162 | 181 |
| P12.5V-6S | 239 | LCZ | 56.45 | 0.04 | 26.69 | 0.22 | 0.07 | 9.26 | 6.17 | 0.56 | 0.02 | 99.48 | 45.3 | 3.2 | 1152 | 170 |
| P12.5V-6S | 264 | LMZ | 58.44 | 0.03 | 25.46 | 0.23 | 0.10 | 7.64 | 6.52 | 1.24 | 0.01 | 99.67 | 39.3 | 7.1 | 964 | 355 |
| P12.5V-2L | 5 | UCZ | 57.20 | 0.06 | 26.79 | 0.23 | 0.12 | 9.44 | 5.76 | 0.55 | 0.02 | 100.18 | 47.5 | 3.2 | 1146 | 182 |
| P16V-3S | 7 | UCZ | 56.36 | 0.06 | 26.88 | 0.22 | 0.16 | 9.43 | 6.01 | 0.56 | 0.02 | 99.70 | 46.4 | 3.2 | 1151 | 172 |
| P16V-3S | 47 | UCZ | 56.04 | 0.06 | 27.02 | 0.28 | 0.25 | 9.44 | 5.94 | 0.58 | 0.02 | 99.63 | 46.8 | 3.3 | 1166 | 181 |
| P16V-3S | 84 | UCZ | 55.93 | 0.06 | 27.10 | 0.25 | 0.17 | 9.51 | 5.90 | 0.56 | 0.02 | 99.50 | 47.1 | 3.2 | 1166 | 177 |
| P16V-3S | 127 | UCZ | 55.99 | 0.06 | 27.07 | 0.28 | 0.23 | 9.50 | 5.96 | 0.56 | 0.02 | 99.67 | 46.8 | 3.2 | 1168 | 173 |
| P16V-3S | 166 | LCZ | 56.12 | 0.05 | 27.00 | 0.21 | 0.27 | 9.52 | 5.92 | 0.55 | 0.02 | 99.66 | 47.1 | 3.1 | 1149 | 160 |
| P16V-3S | 208 | LCZ | 55.88 | 0.04 | 26.77 | 0.19 | 0.27 | 9.27 | 5.94 | 0.63 | 0.01 | 99.00 | 46.3 | 3.6 | 1141 | 187 |
| P16V-3S | 231 | LMZ | 56.27 | 0.04 | 26.83 | 0.21 | 0.26 | 9.33 | 5.93 | 0.64 | 0.02 | 99.53 | 46.5 | 3.7 | 1143 | 194 |
| P16V-8L | 73 | LMZ | 58.55 | 0.04 | 26.35 | 0.27 | 0.15 | 8.48 | 6.19 | 0.74 | 0.01 | 100.79 | 43.1 | 4.3 | 1111 | 227 |
| P00-30C | | UMZ | 58.82 | 0.04 | 25.99 | 0.26 | 0.15 | 8.44 | 5.96 | 1.10 | 0.01 | 100.78 | 43.9 | 6.4 | 1004 | 294 |

[a] An = 100 Ca/(Ca+Na).
[b] Or = 100 K/(Ca+Na+K).

length, commonly with a shape-preferred orientation. Laths may be slightly deformed, displaying bent twinning, undulatory extinction, granulation (primary crystals are replaced by smaller recrystallized grains), and lobate contacts with adjacent minerals, suggesting subsolidus grain boundary adjustment. Similar deformation microstructures have been detailed in the Poe Mountain anorthosite (Wyoming) by Lafrance et al. (1996). Plagioclase commonly contains numerous very small needles of oxide minerals. Some grains also include large equant grains of ilmenite. Plagioclase is undoubtedly a cumulus mineral.

Ilmenite contains lenses of exsolved hematite. It is usually interstitial to the other minerals which

Table 2
Sr isotopic compositions for plagioclase separates from the Tellnes ilmenite deposit

| Sample | Depth | An% | Or% | Rb (ppm) | Sr (ppm) | $^{87}Rb/^{86}Sr$ | $^{87}Sr/^{86}Sr \pm 2\sigma$ (m) | $(^{87}Sr/^{86}Sr)_{920}$ |
|---|---|---|---|---|---|---|---|---|
| P12V-13N | 10 | 46.1 | 3.4 | 0.85 | 1153 | 0.0021 | 0.704503±6 | 0.704475 |
| P12V-3S | 29 | 45.7 | 3.6 | 0.68 | 1142 | 0.0017 | 0.704542±9 | 0.704519 |
| P12V-3S | 87 | 47.3 | 3.0 | 0.78 | 1144 | 0.0020 | 0.704502±7 | 0.704476 |
| P12V-3S | 154 | 46.5 | 3.1 | 0.59 | 1153 | 0.0015 | 0.704492±9 | 0.704473 |
| P12V-3S | 230 | 47.1 | 2.9 | 1.85 | 1182 | 0.0045 | 0.704465±7 | 0.704405 |
| P12V-3S | 285 | 47.7 | 3.6 | 1.54 | 1162 | 0.0038 | 0.704452±7 | 0.704402 |
| P12V-10S | 70 | 46.0 | 3.3 | 0.96 | 1166 | 0.0024 | 0.704478±7 | 0.704447 |
| P12V-14S | 75 | 44.1 | 2.8 | 0.83 | 1133 | 0.0021 | 0.704497±6 | 0.704469 |
| P12V-14S | 96 | 43.2 | 4.6 | 2.21 | 1092 | 0.0059 | 0.704458±6 | 0.704381 |
| P12V-8L | 80 | 46.0 | 4.0 | 1.17 | 1130 | 0.0030 | 0.704439±8 | 0.704400 |
| P12V-8L | 82 | 42.7 | 5.6 | 2.64 | 1051 | 0.0073 | 0.704507±6 | 0.704411 |
| P12.5V-6S | 180 | 47.7 | 3.3 | 1.05 | 1162 | 0.0026 | 0.704427±7 | 0.704393 |
| P12.5V-6S | 239 | 45.3 | 3.2 | 0.85 | 1152 | 0.0021 | 0.704396±6 | 0.704368 |
| P12.5V-6S | 264 | 39.3 | 7.1 | 4.05 | 964 | 0.0122 | 0.704693±7 | 0.704533 |
| P16V-3S | 7 | 46.4 | 3.2 | 0.92 | 1151 | 0.0023 | 0.704520±8 | 0.704490 |
| P16V-3S | 47 | 46.8 | 3.3 | 1.17 | 1166 | 0.0029 | 0.704497±6 | 0.704459 |
| P16V-3S | 84 | 47.1 | 3.2 | 0.80 | 1166 | 0.0020 | 0.704505±6 | 0.704479 |
| P16V-3S | 127 | 46.8 | 3.2 | 0.89 | 1168 | 0.0022 | 0.704464±8 | 0.704435 |
| P16V-3S | 166 | 47.1 | 3.1 | 0.61 | 1149 | 0.0015 | 0.704469±7 | 0.704449 |
| P16V-3S | 208 | 46.3 | 3.6 | 1.18 | 1141 | 0.0030 | 0.704475±6 | 0.704436 |
| P16V-3S | 231 | 46.5 | 3.7 | 1.20 | 1143 | 0.0030 | 0.704487±7 | 0.704447 |

Initial isotopic compositions at 920 Ma.

nevertheless locally contain inclusions of ilmenite. The interstitial habit of ilmenite results from the coalescence of grains with variable orientation and displaying 120° triple junctions. This texture is also due to subsolidus grain boundary migration of primary ilmenite (Hunter, 1996; Duchesne, 1996). Exsolved hematite does not display any deformation, implying that deformation textures in the ore body were acquired above the solvus temperature. As a result of recrystallization, distinction between cumulus and intercumulus ilmenite is difficult. However, the presence of equant ilmenite grains within plagioclase and orthopyroxene shows that ilmenite is a liquidus mineral.

Orthopyroxene is present throughout the ore body but is more abundant in the upper part of the intrusion. Two different textures are observed: (1) subhedral, prismatic grains with well developed Schiller exsolutions (Fig. 5A); (2) smaller anhedral grains that are interstitial to plagioclase (Fig. 5B). In the lower part of the deposit, only interstitial orthopyroxene is observed whereas both textures occur in the upper part. This suggests that orthopyroxene is an intercumulus phase at the base of the deposit and becomes a cumulus phase up-section. Interstitial orthopyroxene reflects crystallization from intercumulus melt.

A small amount of olivine (generally <5%) occurs in the upper part of the ore body. It appears more or less simultaneously with the prismatic orthopyroxene. Only a few samples contain cumulus orthopyroxene without olivine. Olivine is commonly interstitial to the other major minerals but can locally be found included in orthopyroxene. The small proportion of olivine favours an intercumulus character. However, the existence of olivine included in other minerals and its relatively primitive composition (~Fo80, Wilmart et al., 1989) force us to consider olivine as a cumulus phase that appears simultaneously with orthopyroxene. Close to the contact with the anorthosite, olivine has commonly been replaced by symplectitic intergrowths of orthopyroxene and magnetite (Fig. 5C).

Magnetite, clinopyroxene, biotite, apatite and hornblende are considered as intercumulus minerals that crystallized from trapped liquid. This interpretation is based on obvious interstitial, space-filling relationships relative to plagioclase, ilmenite, orthopyroxene and olivine and on their relatively low modal abundances. Grains of clinopyroxene at the margin of orthopyroxene probably represent externally exsolved granules.

Some samples close to the margin with the host anorthosite have unusual textures. The most spectacular is a "dalmatian texture" in which large plagioclase and orthopyroxene oikocrysts enclose numerous, smaller and uniformly distributed ilmenite chadacrysts (Fig. 5E–F). This texture clearly demonstrates the early crystallization of ilmenite. Other marginal rocks (12.5V-6S, 264 and 12V-10S, 64) have a fine-grained texture in which two pyroxenes occur in roughly equal proportions, together with antiperthitic plagioclase, ilmenite and a high proportion of apatite (Fig. 5D). These are interpreted as chills, similar to those of jotunitic dykes (Duchesne et al., 1985, 1989).

Table 3
Whole-rock compositions for major elements (XRF analyses) and mineral proportions (wt.%) of cumulates from the Tellnes ilmenite deposit

| Drill core | Depth | Zone | $SiO_2$ | $TiO_2$ | $Al_2O_3$ | $FeO_{tot}$ | MnO | MgO | CaO | $Na_2O$ | $K_2O$ | $P_2O_5$ | Total | Mg# | Plagio | Ilm | Opx | Olivine | Cpx | Biotite |
|---|---|---|---|---|---|---|---|---|---|---|---|---|---|---|---|---|---|---|---|---|
| 8V-2S | 194 | LCZ | 32.20 | 17.25 | 13.57 | 21.39 | 0.14 | 4.69 | 5.09 | 3.78 | 0.57 | 0.31 | 98.99 | 0.180 | 45.9 | 41.7 | 7.5 | 0.0 | 0.4 | 4.4 |
| 8V-7S | 180 | LCZ | 30.77 | 17.96 | 13.05 | 21.97 | 0.15 | 4.38 | 5.07 | 3.51 | 0.54 | 0.38 | 97.78 | 0.166 | 46.6 | 44.2 | 3.6 | 0.0 | 0.6 | 4.5 |
| 8V-9S | 155 | LCZ | 29.39 | 19.60 | 12.95 | 22.72 | 0.13 | 5.04 | 4.74 | 3.68 | 0.44 | 0.21 | 98.90 | 0.182 | 47.3 | 45.8 | 4.4 | 0.0 | 0.0 | 2.5 |
| 8V-9S | 187 | LCZ | 30.42 | 18.91 | 14.19 | 21.36 | 0.12 | 3.70 | 5.18 | 3.94 | 0.49 | 0.23 | 98.54 | 0.148 | 43.5 | 50.5 | 4.4 | 0.0 | 0.0 | 1.6 |
| 8V-9S | 213 | LCZ | 28.92 | 20.10 | 13.68 | 22.50 | 0.13 | 3.65 | 4.97 | 3.89 | 0.46 | 0.21 | 98.51 | 0.140 | 47.8 | 46.1 | 3.5 | 0.0 | 0.0 | 2.7 |
| 8V-9S | 240 | LCZ | 27.96 | 20.98 | 13.27 | 23.31 | 0.13 | 3.56 | 4.82 | 3.75 | 0.46 | 0.25 | 98.49 | 0.132 | 44.4 | 50.6 | 1.9 | 0.0 | 0.2 | 2.9 |
| 8V-9S | 269 | LCZ | 31.24 | 18.15 | 14.41 | 21.01 | 0.12 | 3.58 | 5.36 | 4.17 | 0.52 | 0.26 | 98.82 | 0.146 | 45.9 | 46.0 | 4.3 | 0.0 | 0.5 | 3.2 |
| 8V-9S | 298 | LCZ | 30.98 | 18.17 | 14.01 | 21.25 | 0.13 | 3.80 | 5.30 | 4.21 | 0.55 | 0.32 | 98.72 | 0.152 | 47.0 | 43.8 | 3.7 | 0.0 | 1.1 | 4.4 |
| 12V-13N | 110 | LCZ | 35.06 | 15.04 | 14.68 | 19.19 | 0.13 | 4.49 | 5.62 | 3.73 | 0.61 | 0.35 | 98.90 | 0.190 | 52.8 | 36.0 | 5.4 | 0.0 | 1.0 | 4.8 |
| 12V-3S | 230 | LCZ | 30.70 | 18.33 | 13.27 | 21.97 | 0.13 | 5.10 | 4.81 | 3.69 | 0.47 | 0.21 | 98.68 | 0.188 | 43.0 | 48.3 | 6.3 | 0.0 | 0.0 | 2.3 |
| 12V-3S | 255 | LCZ | 30.60 | 18.72 | 14.00 | 21.61 | 0.13 | 3.86 | 5.11 | 3.97 | 0.49 | 0.22 | 98.71 | 0.152 | 44.0 | 48.9 | 4.9 | 0.0 | 0.2 | 2.0 |
| 12V-3S | 285 | LCZ | 31.46 | 17.84 | 14.56 | 20.53 | 0.12 | 3.54 | 5.37 | 4.10 | 0.52 | 0.23 | 98.27 | 0.147 | 49.1 | 45.2 | 3.5 | 0.0 | 0.0 | 2.2 |
| 12V-10S | 110 | LCZ | 31.54 | 17.89 | 14.05 | 21.01 | 0.13 | 4.05 | 5.22 | 3.92 | 0.55 | 0.28 | 98.64 | 0.162 | 45.0 | 45.6 | 4.8 | 0.0 | 0.2 | 4.4 |
| 12V-14S | 75 | LCZ | 31.84 | 17.48 | 12.37 | 22.21 | 0.15 | 5.65 | 4.88 | 3.51 | 0.56 | 0.37 | 99.02 | 0.203 | 37.9 | 48.2 | 7.7 | 0.0 | 0.7 | 5.4 |
| 12.5V-6S | 111 | LCZ | 30.98 | 18.36 | 13.99 | 21.11 | 0.12 | 4.03 | 5.12 | 3.68 | 0.49 | 0.23 | 98.11 | 0.160 | 44.0 | 47.0 | 5.4 | 0.0 | 0.3 | 3.3 |
| 12.5V-6S | 153 | LCZ | 30.91 | 18.54 | 13.62 | 21.20 | 0.12 | 3.60 | 5.27 | 4.09 | 0.51 | 0.24 | 98.10 | 0.145 | 50.1 | 43.5 | 3.4 | 0.0 | 0.4 | 2.6 |
| 12.5V-6S | 180 | LCZ | 29.85 | 19.30 | 13.83 | 21.92 | 0.13 | 3.69 | 5.15 | 3.90 | 0.50 | 0.27 | 98.54 | 0.144 | 48.0 | 45.4 | 2.1 | 0.0 | 0.4 | 4.0 |
| 12.5V-6S | 210 | LCZ | 33.17 | 16.53 | 15.03 | 19.54 | 0.12 | 3.66 | 5.61 | 4.15 | 0.62 | 0.33 | 98.76 | 0.158 | 51.2 | 41.5 | 4.8 | 0.0 | 0.7 | 1.8 |
| 12.5V-6S | 239 | LCZ | 32.87 | 16.73 | 14.23 | 20.50 | 0.13 | 4.02 | 5.37 | 4.09 | 0.62 | 0.37 | 98.93 | 0.164 | 47.0 | 45.2 | 3.7 | 0.0 | 0.0 | 4.2 |
| 16V-3S | 166 | LCZ | 31.35 | 18.09 | 13.79 | 21.31 | 0.13 | 4.48 | 5.14 | 3.87 | 0.52 | 0.25 | 98.93 | 0.174 | 45.7 | 45.2 | 4.7 | 0.0 | 0.2 | 4.2 |
| 16V-3S | 208 | LCZ | 30.35 | 18.87 | 13.64 | 22.09 | 0.13 | 3.62 | 5.04 | 3.95 | 0.56 | 0.30 | 98.55 | 0.141 | 50.4 | 42.0 | 3.5 | 0.0 | 0.4 | 3.6 |
| 16V-8L | 5 | LCZ | 31.80 | 17.52 | 13.64 | 21.41 | 0.14 | 4.57 | 5.06 | 3.58 | 0.60 | 0.34 | 98.66 | 0.176 | 43.7 | 43.1 | 7.4 | 0.0 | 0.2 | 5.6 |
| 16V-8L | 30 | LCZ | 33.81 | 16.10 | 14.75 | 19.61 | 0.12 | 3.65 | 5.59 | 3.94 | 0.68 | 0.37 | 98.62 | 0.157 | 48.2 | 42.4 | 4.2 | 0.0 | 1.2 | 4.0 |
| 16V-8L | 51 | LCZ | 37.26 | 13.43 | 15.50 | 17.89 | 0.12 | 4.03 | 5.89 | 4.01 | 0.63 | 0.31 | 99.06 | 0.184 | 49.0 | 38.4 | 9.0 | 0.0 | 0.5 | 3.1 |
| 16V-8L | 68 | LCZ | 34.54 | 15.22 | 13.09 | 20.85 | 0.15 | 5.15 | 5.49 | 3.45 | 0.56 | 0.31 | 98.81 | 0.198 | 36.6 | 42.0 | 8.6 | 0.0 | 0.8 | 11.5 |
| Average of LCZ | | | 31.60 | 17.80 | 13.89 | 21.18 | 0.13 | 4.14 | 5.21 | 3.86 | 0.54 | 0.29 | 98.64 | 0.164 | 46.2 | 44.7 | 4.9 | 0.0 | 0.4 | 3.8 |
| 8V-2S | 210 | LMZ | 33.96 | 15.91 | 14.57 | 19.79 | 0.13 | 3.74 | 5.66 | 4.08 | 0.67 | 0.40 | 98.91 | 0.159 | 50.8 | 40.0 | 3.3 | 0.0 | 1.4 | 4.5 |
| 8V-7S | 140 | LMZ | 31.85 | 17.44 | 13.89 | 21.14 | 0.13 | 3.92 | 5.31 | 3.76 | 0.62 | 0.43 | 98.49 | 0.156 | 47.5 | 40.3 | 7.9 | 0.0 | 0.1 | 4.2 |
| 8V-8S | 90 | LMZ | 33.75 | 15.98 | 13.50 | 20.75 | 0.14 | 4.28 | 5.46 | 3.68 | 0.76 | 0.58 | 98.88 | 0.171 | 50.0 | 38.9 | 1.6 | 0.0 | 0.2 | 9.3 |
| 8V-8S | 120 | LMZ | 36.09 | 14.11 | 14.93 | 18.56 | 0.13 | 3.99 | 5.76 | 4.18 | 0.83 | 0.49 | 99.07 | 0.177 | 47.8 | 38.3 | 8.9 | 0.0 | 0.0 | 5.0 |
| 12V-13N | 140 | LMZ | 41.04 | 9.33 | 17.12 | 15.87 | 0.11 | 3.91 | 6.27 | 4.23 | 0.89 | 0.39 | 99.16 | 0.198 | 62.5 | 25.5 | 4.4 | 0.0 | 0.5 | 2.7 |
| 12V-14S | 47 | LMZ | 39.18 | 11.78 | 16.07 | 16.71 | 0.12 | 3.35 | 6.07 | 4.50 | 0.95 | 0.49 | 99.22 | 0.167 | 58.1 | 32.3 | 4.1 | 0.0 | 2.5 | 3.1 |
| 12V-14S | 96 | LMZ | 40.29 | 10.67 | 15.57 | 16.40 | 0.13 | 4.65 | 6.19 | 4.07 | 0.87 | 0.51 | 99.35 | 0.221 | 52.7 | 34.8 | 6.8 | 0.0 | 0.7 | 4.5 |
| 12.5V-6S | 264 | LMZ | 46.84 | 5.39 | 16.10 | 13.07 | 0.14 | 5.18 | 7.15 | 4.10 | 1.07 | 0.69 | 99.73 | 0.284 | 55.5 | 15.1 | 12.6 | 0.0 | 9.8 | 5.0 |
| 16V-6N | 57 | LMZ | 36.16 | 13.59 | 14.35 | 18.80 | 0.13 | 5.01 | 5.61 | 3.90 | 0.67 | 0.48 | 98.70 | 0.210 | 48.1 | 34.2 | 9.8 | 0.0 | 2.3 | 5.0 |
| 16V-3S | 231 | LMZ | 33.17 | 16.59 | 14.44 | 20.13 | 0.13 | 3.57 | 5.49 | 4.11 | 0.66 | 0.40 | 98.69 | 0.151 | 49.1 | 39.8 | 5.1 | 0.0 | 1.6 | 4.4 |
| 16V-4S | 103 | LMZ | 42.53 | 9.00 | 16.66 | 14.28 | 0.11 | 4.89 | 6.42 | 4.08 | 0.78 | 0.36 | 99.11 | 0.255 | 57.3 | 29.6 | 5.0 | 0.0 | 2.6 | 5.1 |
| 16V-8L | 73 | LMZ | 40.85 | 10.01 | 16.41 | 15.68 | 0.11 | 4.19 | 6.27 | 4.14 | 0.88 | 0.42 | 98.96 | 0.211 | 52.9 | 33.0 | 5.3 | 0.0 | 4.3 | 4.5 |
| 16V-8L | 74 | LMZ | 33.94 | 15.03 | 12.27 | 23.01 | 0.18 | 5.14 | 5.15 | 3.09 | 0.53 | 0.33 | 98.67 | 0.183 | 39.8 | 42.9 | 7.8 | 0.0 | 5.0 | 3.8 |

| | | | | | | | | | | | | | | | | | | | | |
|---|---|---|---|---|---|---|---|---|---|---|---|---|---|---|---|---|---|---|---|---|
| Average of LMZ | | | 37.67 | 12.68 | 15.07 | 18.01 | 0.13 | 4.29 | 5.91 | 3.99 | 0.78 | 0.46 | 99.00 | 0.196 | 51.7 | 34.2 | 6.4 | 0.0 | 2.4 | 4.7 |
| 8V-4N | 210 | UCZ | 32.16 | 17.16 | 12.89 | 21.69 | 0.14 | 6.26 | 4.77 | 3.48 | 0.46 | 0.23 | 99.24 | 0.224 | 41.8 | 42.0 | 7.9 | 2.0 | 2.1 | 3.2 |
| 8V-4N | 238 | UCZ | 29.76 | 19.04 | 12.58 | 23.11 | 0.14 | 5.50 | 4.59 | 3.53 | 0.44 | 0.23 | 98.92 | 0.192 | 45.8 | 43.1 | 4.8 | 2.5 | 0.1 | 3.2 |
| 8V-5N | 77 | UCZ | 32.50 | 17.06 | 11.12 | 23.17 | 0.17 | 7.74 | 4.20 | 2.97 | 0.42 | 0.21 | 99.56 | 0.250 | 33.7 | 39.0 | 18.3 | 1.8 | 0.9 | 2.6 |
| 8V-5N | 113 | UCZ | 31.87 | 17.47 | 11.62 | 22.87 | 0.16 | 7.21 | 4.30 | 3.14 | 0.49 | 0.25 | 99.38 | 0.240 | 29.9 | 42.6 | 20.1 | 1.2 | 0.9 | 4.0 |
| 8V-6N | 17 | UCZ | 33.55 | 16.79 | 10.42 | 23.77 | 0.18 | 7.10 | 3.99 | 2.59 | 0.62 | 0.33 | 99.34 | 0.230 | 24.5 | 38.5 | 27.0 | 1.1 | 0.1 | 4.3 |
| 8V-6N | 40 | UCZ | 35.51 | 15.09 | 11.91 | 21.34 | 0.16 | 6.20 | 4.62 | 2.98 | 0.76 | 0.41 | 98.98 | 0.225 | 35.6 | 39.8 | 18.4 | 0.5 | 1.2 | 4.6 |
| 8V-2S | 16 | UCZ | 34.61 | 14.88 | 8.65 | 24.89 | 0.21 | 10.11 | 3.57 | 2.18 | 0.53 | 0.35 | 99.98 | 0.289 | 24.5 | 38.5 | 27.8 | 0.3 | 0.1 | 4.3 |
| 8V-2S | 65 | UCZ | 34.31 | 16.08 | 11.19 | 22.33 | 0.15 | 6.95 | 4.27 | 3.02 | 0.65 | 0.35 | 99.30 | 0.237 | 37.8 | 36.7 | 20.8 | 0.4 | 0.0 | 4.4 |
| 8V-2S | 120 | UCZ | 34.80 | 15.60 | 12.36 | 21.17 | 0.15 | 6.18 | 4.65 | 3.41 | 0.66 | 0.33 | 99.28 | 0.226 | 37.3 | 39.6 | 18.3 | 0.4 | 0.5 | 3.3 |
| 8V-2S | 158 | UCZ | 33.23 | 16.37 | 12.94 | 21.39 | 0.14 | 5.91 | 4.82 | 3.55 | 0.58 | 0.35 | 99.28 | 0.216 | 43.2 | 39.2 | 8.3 | 2.8 | 0.2 | 4.7 |
| 8V-9S | 44 | UCZ | 35.61 | 15.01 | 11.88 | 21.50 | 0.17 | 7.23 | 4.36 | 3.14 | 0.47 | 0.18 | 99.55 | 0.252 | 37.7 | 36.8 | 22.8 | 0.0 | 0.1 | 2.6 |
| 8V-9S | 70 | UCZ | 35.30 | 14.86 | 13.57 | 19.89 | 0.14 | 6.40 | 4.95 | 3.50 | 0.51 | 0.22 | 99.34 | 0.243 | 39.2 | 41.3 | 13.6 | 0.0 | 0.2 | 4.0 |
| 8V-9S | 100 | UCZ | 29.07 | 19.61 | 11.92 | 23.75 | 0.15 | 6.01 | 4.35 | 3.30 | 0.42 | 0.21 | 98.78 | 0.202 | 41.8 | 41.3 | 7.9 | 3.1 | 0.1 | 5.2 |
| 8V-9S | 130 | UCZ | 29.37 | 19.27 | 12.41 | 23.27 | 0.14 | 5.75 | 4.53 | 3.69 | 0.43 | 0.22 | 99.08 | 0.198 | 40.9 | 45.9 | 6.9 | 2.3 | 0.0 | 3.6 |
| 8.2V-9S | 34 | UCZ | 29.36 | 19.43 | 9.10 | 26.09 | 0.19 | 8.56 | 3.56 | 2.24 | 0.35 | 0.26 | 99.14 | 0.247 | 28.9 | 48.3 | 16.4 | 3.3 | 0.5 | 2.5 |
| 8.2V-9S | 69 | UCZ | 31.97 | 17.07 | 12.20 | 22.42 | 0.15 | 7.01 | 4.51 | 3.04 | 0.46 | 0.22 | 99.05 | 0.238 | 38.2 | 43.2 | 10.1 | 4.1 | 0.4 | 3.1 |
| 11.5V-5S | 97 | UCZ | 29.92 | 18.88 | 12.32 | 22.97 | 0.14 | 5.79 | 4.51 | 3.18 | 0.44 | 0.24 | 98.39 | 0.201 | 44.7 | 41.5 | 5.4 | 3.0 | 0.1 | 4.5 |
| 11.5V-5S | 124 | UCZ | 30.48 | 18.60 | 13.17 | 21.93 | 0.13 | 5.02 | 4.95 | 3.45 | 0.46 | 0.23 | 98.42 | 0.186 | 45.6 | 44.0 | 7.1 | 0.2 | 0.0 | 3.0 |
| 12V-13N | 10 | UCZ | 33.71 | 15.62 | 12.81 | 21.23 | 0.15 | 6.88 | 4.76 | 3.41 | 0.50 | 0.24 | 99.31 | 0.245 | 40.4 | 38.5 | 13.7 | 2.6 | 0.1 | 3.1 |
| 12V-13N | 34 | UCZ | 31.34 | 17.47 | 12.02 | 22.92 | 0.15 | 6.84 | 4.44 | 3.09 | 0.45 | 0.25 | 98.97 | 0.230 | 37.8 | 40.6 | 10.2 | 6.3 | 1.3 | 2.9 |
| 12V-13N | 59 | UCZ | 32.71 | 16.59 | 12.78 | 21.56 | 0.14 | 6.70 | 4.74 | 3.24 | 0.51 | 0.26 | 99.22 | 0.237 | 44.4 | 40.4 | 4.4 | 6.0 | 0.2 | 3.9 |
| 12V-3S | 29 | UCZ | 35.24 | 14.42 | 12.65 | 20.72 | 0.15 | 7.74 | 4.66 | 3.26 | 0.53 | 0.23 | 99.60 | 0.272 | 40.7 | 36.5 | 13.7 | 3.6 | 0.3 | 4.6 |
| 12V-3S | 54 | UCZ | 29.46 | 19.17 | 10.28 | 25.05 | 0.17 | 8.32 | 3.76 | 2.74 | 0.35 | 0.16 | 99.46 | 0.249 | 35.7 | 43.0 | 12.5 | 5.1 | 0.0 | 2.2 |
| 12V-3S | 87 | UCZ | 29.62 | 18.94 | 10.70 | 24.67 | 0.16 | 7.81 | 3.91 | 2.88 | 0.38 | 0.19 | 99.26 | 0.240 | 35.5 | 46.4 | 7.5 | 5.3 | 0.2 | 4.2 |
| 12V-3S | 120 | UCZ | 32.28 | 16.93 | 12.10 | 22.26 | 0.15 | 7.19 | 4.49 | 3.29 | 0.49 | 0.24 | 99.42 | 0.244 | 39.4 | 41.4 | 10.8 | 3.3 | 0.4 | 3.7 |
| 12V-3S | 154 | UCZ | 31.17 | 17.79 | 11.83 | 23.00 | 0.15 | 6.98 | 4.38 | 3.24 | 0.47 | 0.24 | 99.25 | 0.233 | 40.6 | 40.4 | 10.0 | 3.5 | 0.4 | 4.5 |
| 12V-3S | 194 | UCZ | 30.90 | 18.13 | 12.29 | 22.75 | 0.15 | 6.40 | 4.53 | 3.38 | 0.44 | 0.22 | 99.19 | 0.220 | 40.7 | 41.8 | 10.1 | 2.0 | 0.5 | 3.2 |
| 12V-9S | 45 | UCZ | 38.20 | 11.20 | 14.45 | 19.77 | 0.13 | 6.14 | 5.50 | 3.31 | 0.61 | 0.22 | 99.54 | 0.237 | 42.5 | 34.4 | 13.5 | 2.1 | 1.5 | 5.3 |
| 12V-9S | 77 | UCZ | 31.57 | 17.39 | 12.59 | 22.55 | 0.15 | 6.26 | 4.71 | 3.38 | 0.45 | 0.20 | 99.25 | 0.217 | 42.7 | 41.2 | 8.3 | 3.9 | 0.4 | 1.9 |
| 12V-10S | 70 | UCZ | 37.25 | 12.32 | 14.76 | 18.71 | 0.12 | 6.16 | 5.48 | 3.74 | 0.57 | 0.23 | 99.34 | 0.248 | 47.8 | 31.5 | 8.9 | 3.4 | 1.1 | 3.9 |
| 12V-7L | 10 | UCZ | 30.63 | 18.19 | 11.07 | 23.72 | 0.16 | 7.52 | 4.09 | 2.96 | 0.43 | 0.21 | 98.98 | 0.241 | 34.9 | 42.8 | 12.8 | 5.2 | 0.3 | 2.4 |
| 12V-7L | 47 | UCZ | 34.50 | 15.41 | 13.82 | 20.07 | 0.14 | 4.91 | 5.26 | 3.88 | 0.67 | 0.39 | 99.05 | 0.197 | 48.3 | 35.7 | 10.0 | 0.3 | 0.8 | 4.6 |
| 12V-8L | 3 | UCZ | 30.34 | 18.53 | 11.15 | 23.98 | 0.16 | 7.49 | 4.10 | 2.98 | 0.40 | 0.20 | 99.33 | 0.238 | 35.9 | 45.4 | 13.0 | 2.7 | 0.2 | 2.1 |
| 12V-8L | 40 | UCZ | 32.24 | 16.95 | 12.92 | 21.65 | 0.14 | 5.79 | 4.82 | 3.37 | 0.53 | 0.30 | 98.71 | 0.211 | 44.5 | 38.8 | 7.0 | 2.4 | 2.2 | 4.0 |
| 12.5V-6S | 47 | UCZ | 31.26 | 17.87 | 12.45 | 22.50 | 0.15 | 6.23 | 4.61 | 3.18 | 0.46 | 0.24 | 98.95 | 0.217 | 35.7 | 50.2 | 7.6 | 3.4 | 0.7 | 2.5 |
| 12.5V-6S | 79 | UCZ | 29.07 | 19.61 | 12.37 | 23.56 | 0.14 | 5.70 | 4.47 | 3.20 | 0.41 | 0.20 | 98.73 | 0.195 | 40.7 | 47.9 | 6.3 | 1.3 | 0.6 | 2.6 |
| 12.5V-2L | 5 | UCZ | 30.56 | 18.08 | 10.58 | 24.34 | 0.16 | 8.49 | 3.88 | 2.75 | 0.40 | 0.20 | 99.44 | 0.259 | 30.4 | 46.9 | 13.3 | 6.0 | 1.0 | 2.1 |
| 13V-8L | 5 | UCZ | 36.64 | 13.36 | 13.56 | 19.37 | 0.14 | 7.16 | 5.07 | 3.51 | 0.53 | 0.28 | 99.62 | 0.270 | 45.7 | 34.9 | 12.1 | 2.3 | 0.7 | 4.2 |
| 16V-6N | 15 | UCZ | 33.01 | 15.94 | 12.72 | 21.78 | 0.15 | 6.53 | 4.82 | 3.46 | 0.52 | 0.32 | 99.25 | 0.231 | 44.0 | 39.7 | 8.6 | 3.0 | 0.4 | 2.6 |
| 16V-3S | 7 | UCZ | 32.14 | 16.73 | 11.94 | 22.47 | 0.15 | 7.21 | 4.41 | 3.18 | 0.47 | 0.22 | 98.92 | 0.243 | 31.8 | 42.8 | 17.7 | 4.2 | 0.1 | 2.8 |
| 16V-3S | 47 | UCZ | 32.24 | 16.83 | 12.34 | 22.13 | 0.15 | 6.99 | 4.59 | 3.29 | 0.47 | 0.23 | 99.26 | 0.240 | 38.8 | 41.1 | 12.4 | 3.3 | 0.3 | 3.2 |
| 16V-3S | 84 | UCZ | 30.96 | 17.74 | 12.08 | 22.94 | 0.15 | 6.95 | 4.43 | 3.26 | 0.42 | 0.21 | 99.14 | 0.233 | 42.2 | 40.1 | 8.9 | 3.5 | 0.4 | 3.5 |
| 16V-3S | 127 | UCZ | 30.91 | 18.16 | 12.76 | 22.34 | 0.14 | 5.91 | 4.68 | 3.51 | 0.46 | 0.22 | 99.09 | 0.209 | 45.7 | 43.0 | 5.5 | 1.9 | 0.1 | 3.2 |
| 16V-4S | 6 | UCZ | 32.82 | 16.22 | 12.42 | 21.89 | 0.15 | 7.05 | 4.64 | 3.32 | 0.50 | 0.23 | 99.24 | 0.244 | 37.3 | 42.2 | 8.8 | 5.9 | 1.3 | 2.1 |

*(continued on next page)*

Table 3 (*continued*)

| Drill core | Depth | Zone | $SiO_2$ | $TiO_2$ | $Al_2O_3$ | $FeO_{tot}$ | MnO | MgO | CaO | $Na_2O$ | $K_2O$ | $P_2O_5$ | Total | Mg# | Plagio | Ilm | Opx | Olivine | Cpx | Biotite |
|---|---|---|---|---|---|---|---|---|---|---|---|---|---|---|---|---|---|---|---|---|
| 16V-4S | 25 | UCZ | 26.72 | 21.66 | 9.11 | 27.04 | 0.18 | 8.18 | 3.31 | 2.48 | 0.33 | 0.20 | 99.21 | 0.232 | 33.4 | 47.7 | 10.2 | 3.2 | 0.5 | 4.0 |
| 16V-4S | 65 | UCZ | 30.80 | 18.23 | 12.37 | 22.83 | 0.15 | 5.79 | 4.64 | 3.44 | 0.47 | 0.24 | 98.96 | 0.202 | 41.1 | 43.2 | 8.6 | 1.7 | 0.9 | 2.4 |
| Average of UCZ | | | 32.21 | 17.04 | 12.07 | 22.51 | 0.15 | 6.79 | 4.49 | 3.20 | 0.49 | 0.25 | 99.19 | 0.231 | 38.9 | 41.3 | 11.9 | 2.7 | 0.5 | 3.5 |
| 7.8V-1N | 7 | UMZ | 36.79 | 13.26 | 14.06 | 19.14 | 0.14 | 5.36 | 5.45 | 3.95 | 0.76 | 0.50 | 99.41 | 0.219 | 40.3 | 32.9 | 18.2 | 0.0 | 3.2 | 3.0 |
| 8V-4N | 156 | UMZ | 37.31 | 12.85 | 13.92 | 19.17 | 0.14 | 6.33 | 5.37 | 3.58 | 0.55 | 0.31 | 99.53 | 0.248 | 50.4 | 28.1 | 15.3 | 0.0 | 2.1 | 3.1 |
| 8V-6N | 67 | UMZ | 38.60 | 12.17 | 14.83 | 17.53 | 0.13 | 4.95 | 5.69 | 3.80 | 0.85 | 0.45 | 99.00 | 0.220 | 47.0 | 31.1 | 10.9 | 0.0 | 3.3 | 6.5 |
| 8.2V-9S | 11 | UMZ | 40.88 | 9.89 | 14.43 | 17.94 | 0.13 | 6.12 | 5.45 | 3.34 | 0.72 | 0.26 | 99.14 | 0.254 | 48.8 | 28.9 | 18.5 | 0.0 | 1.3 | 2.5 |
| 12V-2N | 104 | UMZ | 40.85 | 10.43 | 15.20 | 16.30 | 0.13 | 5.36 | 5.94 | 4.02 | 0.82 | 0.38 | 99.43 | 0.247 | 54.6 | 28.4 | 10.1 | 0.0 | 1.5 | 4.8 |
| 12V-7N | 46 | UMZ | 40.73 | 10.33 | 15.47 | 16.01 | 0.12 | 5.06 | 6.09 | 4.01 | 0.78 | 0.38 | 98.98 | 0.240 | 55.2 | 27.9 | 7.4 | 0.0 | 0.9 | 8.5 |
| 12V-7L | 71 | UMZ | 40.17 | 10.17 | 14.41 | 17.69 | 0.14 | 5.94 | 6.05 | 3.69 | 0.81 | 0.40 | 99.47 | 0.251 | 51.7 | 32.8 | 12.5 | 0.0 | 1.0 | 1.4 |
| 12V-8L | 80 | UMZ | 40.54 | 10.42 | 15.80 | 15.97 | 0.12 | 5.25 | 6.02 | 3.93 | 0.66 | 0.23 | 98.94 | 0.247 | 52.7 | 30.7 | 11.5 | 0.0 | 2.3 | 2.8 |
| 12V-8L | 82 | UMZ | 41.75 | 9.69 | 15.60 | 15.65 | 0.12 | 4.93 | 6.22 | 4.06 | 0.93 | 0.46 | 99.41 | 0.240 | 51.5 | 26.5 | 13.8 | 0.0 | 4.4 | 3.5 |
| 00-30C | | UMZ | 39.06 | 10.95 | 14.38 | 17.82 | 0.14 | 5.09 | 5.79 | 4.65 | 1.14 | 0.57 | 99.59 | 0.222 | 50.9 | 32.7 | 5.7 | 0.0 | 3.9 | 5.8 |
| Average of UMZ | | | 39.67 | 11.02 | 14.81 | 17.32 | 0.13 | 5.44 | 5.81 | 3.90 | 0.80 | 0.39 | 99.29 | 0.239 | 50.3 | 30.0 | 12.4 | 0.0 | 2.4 | 4.2 |

### *5.2. Modal proportions and spatial variations in cumulus mineralogy*

Our petrographical study confirms the variations of modal proportions previously described by Gierth and Krause (1973) and reveals systematic variations in the cumulus assemblage throughout the deposit. The zoning is observed in each of the three sections studied (800, 1200 and 1600), suggesting that variations along the length of the ore body are not significant.

Based on the modal and textural variations, the four zones identified by Kullerud (2003) on the basis of mining whole-rock data have been defined in the three sections (Fig. 6): (1) the Lower Central Zone (LCZ); (2) the Upper Central Zone (UCZ); (3) the Upper Marginal Zone (UMZ) and (4) the Lower Marginal Zone (LMZ). As detailed later, the Tellnes ilmenite deposit is interpreted as a sill-like body that has subsided so that it has now a synclinal shape. The original morphology and spatial distribution of the different zones has been therefore strongly modified by later deformation.

The Lower Central Zone (LCZ) represents rocks from the lower part of the ore body and also the upper south part in sections 800 and 1200. In the LCZ, plagioclase and ilmenite constitute ~90% of the mode and are the only cumulus phases (pi-C). Their average amounts are 46.2 and 44.7 wt.% respectively. It is the most ilmenite-rich part of the deposit. Orthopyroxene is also present but in minor amounts as small interstitial grains. Olivine and large grains of magnetite are absent. Magnetite is only present as rare small grains associated with sulphides. Other intercumulus minerals are biotite, apatite, clinopyroxene and locally amphibole.

The Upper Central Zone (UCZ) comprises the upper portion of the intrusion, excluding the marginal rocks. Plagioclase, ilmenite, orthopyroxene and olivine are the cumulus minerals (piho-C) with average amounts of respectively 38.9, 41.3, 11.9 and 2.7 wt.%. The orthopyroxene content increases upwards through the UCZ. Intercumulus magnetite is invariably present. Clinopyroxene, biotite, apatite and locally amphibole are also intercumulus phases. The boundary between the UCZ and LCZ is well defined as olivine and large crystals of prismatic orthopyroxene appear together. This boundary has a trough-shape and is grossly parallel in section to the bottom of the ore body.

The Upper Marginal Zone (UMZ) is situated at the margins of the ore body between the UCZ and the contact with the host anorthosite. It is characterized by a higher abundance of plagioclase (50.3 wt.% on average) and apatite, and a lower content of ilmenite (30.0 wt.%

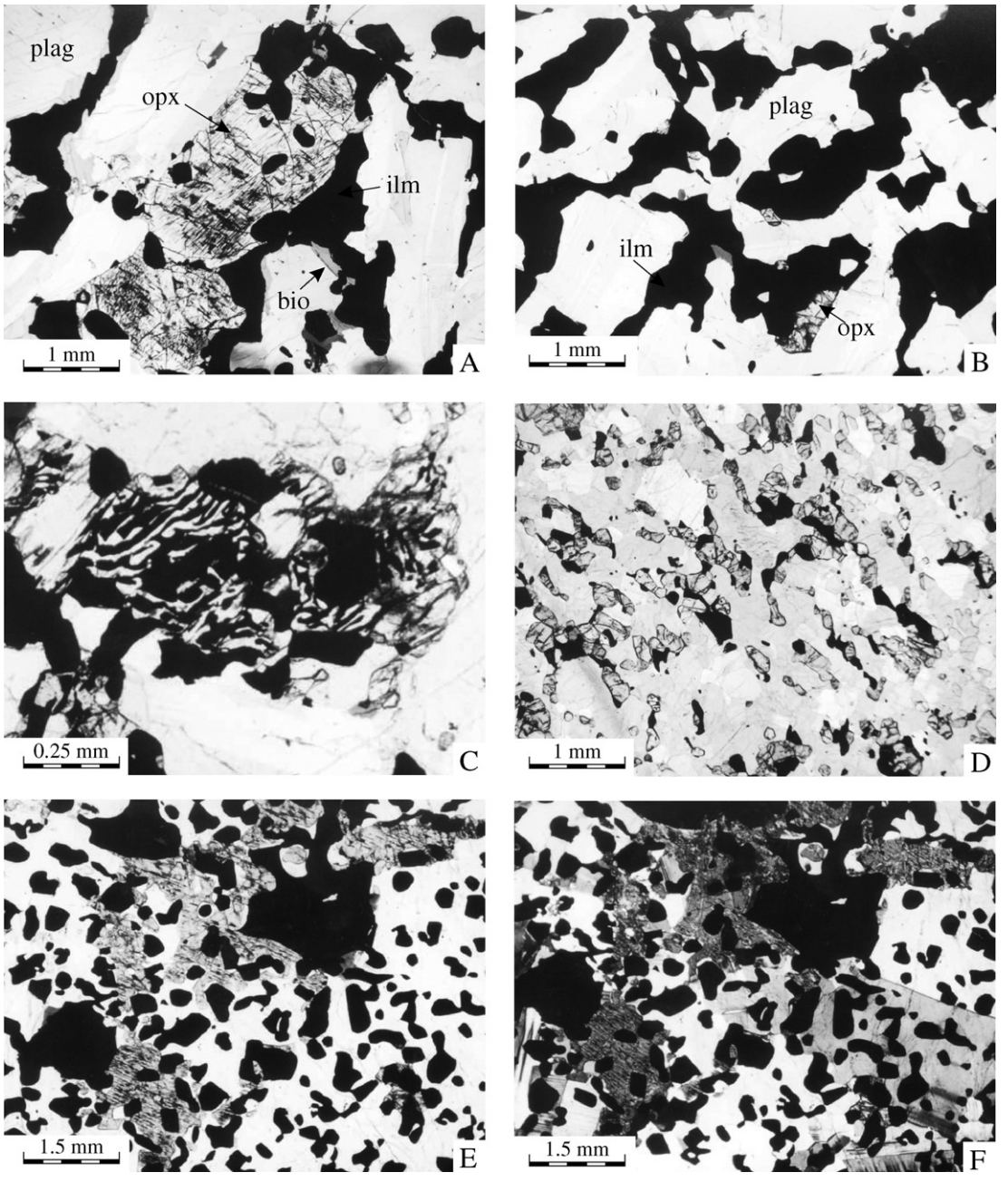


Fig. 5. Microphotographs showing the main textures observed in the Tellnes ilmenite deposit. A. Large prismatic orthopyroxene with Schiller exsolutions, with ilmenite inclusions. Larger ilmenite grains have interstitial morphologies, wrapping orthopyroxene and plagioclase laths. Traces of biotite are common (sample 8V-4N, 156; UCZ); B. Small anhedral orthopyroxene interstitial to plagioclase. Note lobate contacts between plagioclase and ilmenite (sample 12V-3S, 255; LCZ); C. Symplectitic intergrowths of orthopyroxene and oxides replacing primary olivine (sample T2 from Diot et al., 2003; UMZ); D. Fine-grained jotunite with the two pyroxenes in similar proportions, antiperthitic plagioclase, ilmenite and relatively large proportion of apatite (sample 12V-10S, 64; UMZ); E: Poikilitic texture with large plagioclase and pyroxene oikocrysts enclosing numerous small ilmenite chadacrysts giving a "Dalmatian texture" (sample 99-24 b, NE margin of the ore body; UMZ); F: same view under crossed nicols.

on average) than the UCZ. Magnetite is present and clinopyroxene forms relatively abundant subhedral grains. Symplectitic intergrowths of orthopyroxene and ilmenite/magnetite are common and resulted from the oxidation of cumulus olivine. The thickness of the UMZ is about 15 to 20 m and the transition to the UCZ

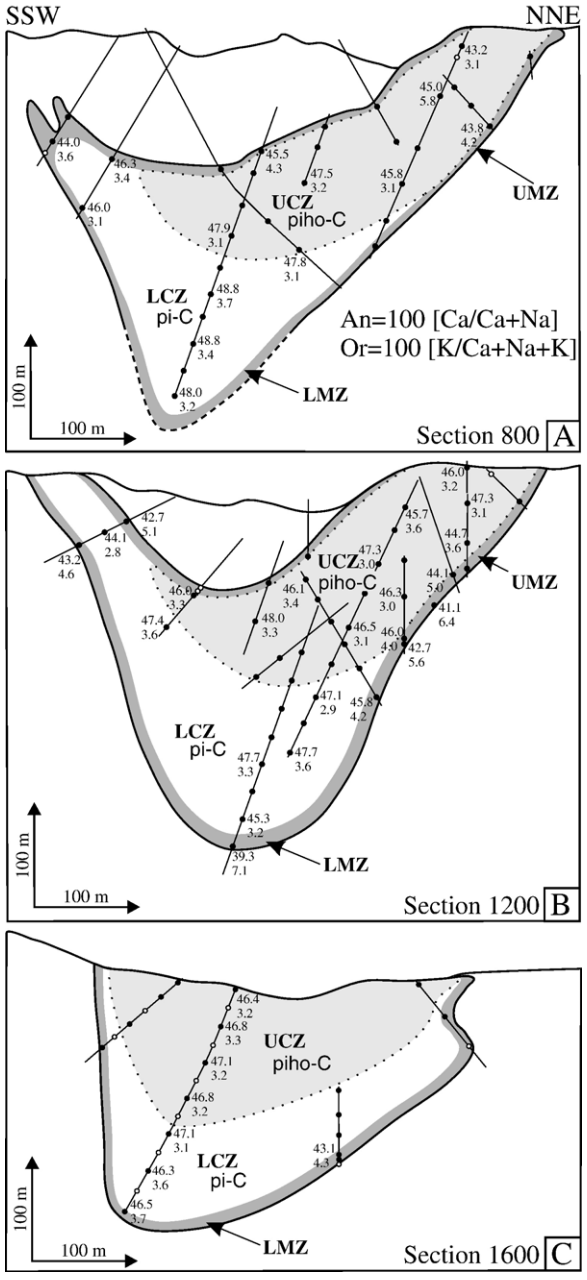


Fig. 6. (A–C) Cross sections (800, 1200 and 1600) through the Tellnes ilmenite deposit showing the spatial distribution of different zones and plagioclase compositions (An and Or content) in selected samples. LCZ=Lower Central Zone; UCZ=Upper Central Zone; UMZ=Upper Marginal Zone; LMZ=Lower Marginal Zone; p=plagioclase; i=ilmenite; h=orthopyroxene; o=olivine; -C=cumulate. Cumulate nomenclature after Irvine (1982).

is gradational and characterized by a decrease in the proportion of plagioclase to ilmenite. The UMZ is absent in section 1600 because the margins of the ore body are only in contact with the LCZ.

The Lower Marginal Zone (LMZ) is situated between the LCZ and the contact. It is similar to the UMZ: relatively plagioclase-rich and ilmenite-poor (51.2 and 34.4 wt.% respectively). However, symplectitic intergrowths are absent (due to the absence of olivine in the primary assemblage) and orthopyroxene is less abundant. As with the UMZ, apatite is more abundant than in the LCZ.

## 6. Analytical results

### 6.1. Plagioclase compositions

Plagioclase compositions are widely used to characterize stratigraphic variations (cryptic layering) in cumulates in layered intrusions in order to identify magma chamber processes such as fractional crystallization, magma recharge, assimilation or trapped liquid crystallization. Even though plagioclase is known to retain its primary composition as a result of slow NaSi–CaAl exchange (Grove et al., 1981), reequilibration and diffusion could nevertheless be significant in deep-seated plutonic rocks. Deformed twinning and local polygonization are common in Tellnes though less extensive than in other nearby intrusions such as Bjerkreim-Sokndal and the anorthosite massifs. This weak granulation is possibly due to the relatively ductile behaviour of ilmenite which has absorbed most of the strain. Nevertheless, recrystallization of primary euhedral laths of plagioclase might have overprinted and blurred any original plagioclase zoning. In order to eliminate the variations resulting from recrystallization of zoned crystals, we have characterized the plagioclase by its bulk composition rather than by using a microprobe.

Previous data on plagioclase from Wilmart et al. (1989) described it as having a composition in the range $An_{45–39}$. Compositions $An_{45–42}$ were reported in the centre of the ore body and, more sodic plagioclase (down to $An_{39}$) occurred in some apophyses and in plagioclase-rich rocks at the margins. The new data reveal a larger range of compositions than previously described (Table 1). Bulk plagioclase compositions vary from $An_{48.8}$ to $An_{39.3}$ (An=100 [Ca/Ca+Na]) and $Or_{2.8}$ to $Or_{7.1}$ (Or=100 [K/Ca+Na+K]). Iron in plagioclase has been shown to be a monitor of magma composition (e.g. Tegner, 1997) and an indicator of the oxygen fugacity (Phinney, 1992). However, our analyses on mineral separates do not allow us to make detailed investigation of the iron content of plagioclase as it contains numerous small oxide inclusions. MgO, $TiO_2$ and MnO are minor components that are very sensitive

to contamination and their variations will not be considered.

Spatial variations of An and Or content in plagioclase are shown in Fig. 6. Compositions are relatively constant in the LCZ and UCZ (~$An_{49–45}$). The major variation in plagioclase composition is observed at the margins of the ore body where an abrupt decrease in An ($An_{43–39}$) and increase in Or ($Or_{4–7}$) is commonly observed.

Sr and Ba (Table 1) have also been analysed in plagioclase separates. Sr is compatible in plagioclase (see Vander Auwera et al., 2000 for a review) whereas Ba is incompatible (Bindeman et al., 1998). The range of variation is quite small for Sr (964 to 1182 ppm) and more significant for Ba (154 to 355 ppm). The Sr content is higher in samples from LCZ and UCZ whereas samples from LMZ and UMZ are comparatively enriched in Ba. Binary diagrams (Fig. 7) show that An and Sr (compatible behaviour) are positively correlated. Or and Ba (incompatible behaviour) are correlated positively and negatively with An and Sr. These trends do not result from variations of partition coefficients for Sr and Ba because they increase linearly with decreasing An content (Bindeman et al., 1998). This is evident from the An–Sr relation which is opposite to the trend predicted by variations in partition coefficients. On the other hand, it is clear that these trends are closely related to the $P_2O_5$ content in the bulk cumulate. $P_2O_5$-richer cumulates have plagioclase with higher Or and Ba contents while $P_2O_5$-poorer samples have plagioclase with higher An and Sr contents.

### 6.2. Sr isotope geochemistry

Sr isotopic ratios and Rb and Sr concentrations have been analysed for 21 separated plagioclases (Table 2). Measured $^{87/86}Sr$ ratios display a very restricted range (0.704396–0.704693). These values are slightly lower than data reported by Wilmart et al. (1989) on four bulk cumulates from the ore body (0.70487–0.70510). They correspond to the lowest values in the Rogaland Anorthosite Province (see Bolle et al., 2003, for a review). The spatial variability of $^{87/86}Sr_{(920)}$ is shown in Fig. 8. Systematic variations of this ratio are observed in section 1200 (Fig. 8A). The lowest $^{87/86}Sr_{(920)}$ ratio (0.704368) is found at the base of the section and it increases continuously towards the top, where it reaches 0.704519. Sample 12.5V-6S (264), situated 10 cm from the contact with the host anorthosite, displays the highest ratio (0.704533). Values for $^{87/86}Sr_{(920)}$ in section 1600 (Fig. 8B) are in the same range as values in the upper part of section 1200. The range of variation is minor, unsystematic, and probably not genetically significant.

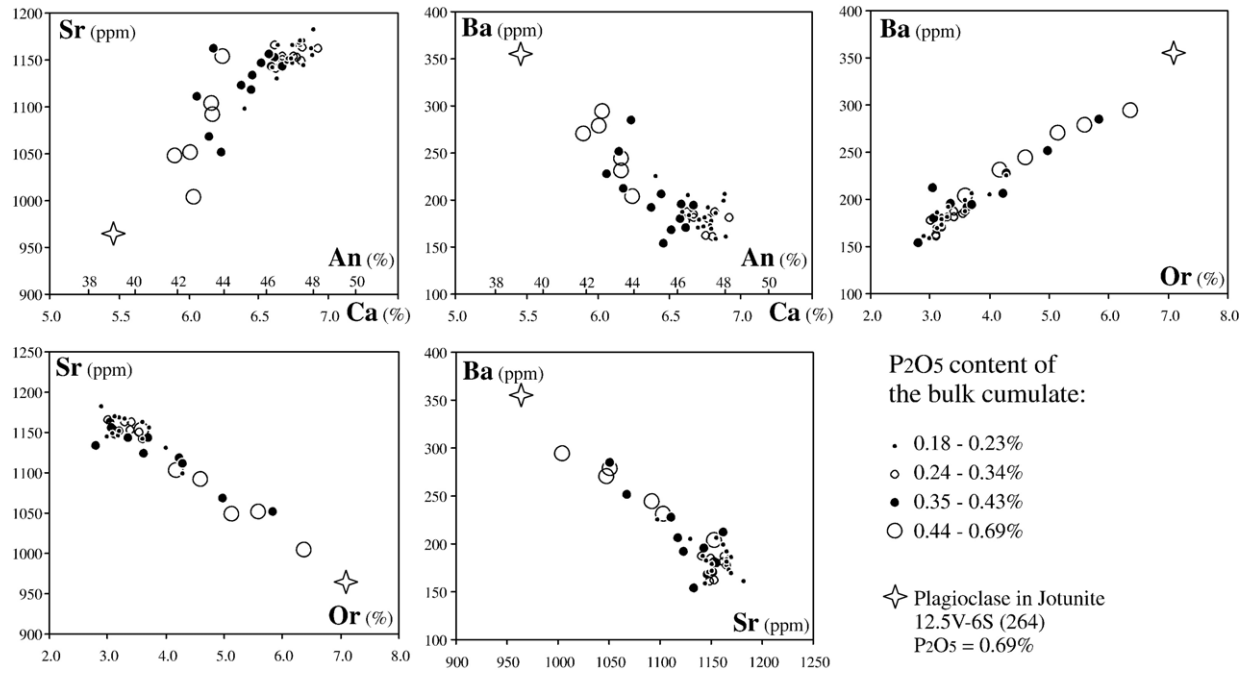


Fig. 7. Binary diagrams for plagioclase composition from the Tellnes ilmenite deposit. Symbols are related to a range of $P_2O_5$ contents in the bulk cumulate.

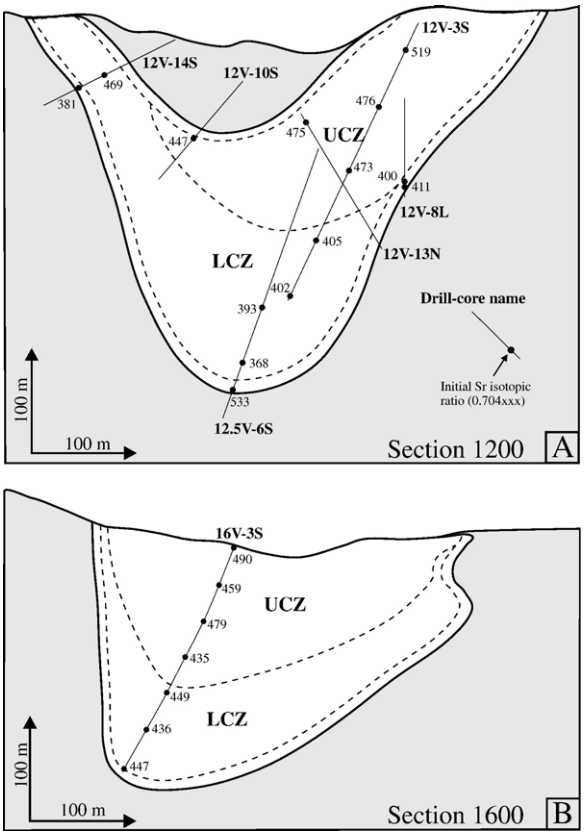


Fig. 8. Spatial distribution of $^{87/86}Sr_{(920)}$ in plagioclase from cross section 1200 and 1600 and location of the LCZ and UCZ in the Tellnes ilmenite deposit. Only the three last decimals of the ratios are indicated.

### 6.3. Whole-rock compositions

Ninety seven new whole-rock analyses (Table 3) are plotted in major element binary diagrams (Fig. 9) together with mining data. $SiO_2$ and $TiO_2$ have been chosen as variation indices, as $SiO_2$ is essentially correlated with the modal abundance of plagioclase and orthopyroxene and $TiO_2$ reflects the amount of ilmenite. The distribution of the new analyses mimics the variation of mining data, except for some plagioclase-rich samples from the mining database. These plagioclase-rich samples consist of mixtures of the ore and the host anorthosite or anorthositic xenoliths and are thus not representative of rocks from the Tellnes ilmenite deposit.

Compositional ranges of cumulus minerals (plagioclase, ilmenite, orthopyroxene and olivine) are represented by a circle or indicated by an arrow. One of the rock samples from the LMZ (jot) has been circled. This sample 12.5V-6S (264) has the lowest $TiO_2$ and $FeO_{tot}$ and the highest $SiO_2$ and CaO of our suite of samples. It is also characterized by the highest $P_2O_5$ (0.69%, Table 3). The texture (Fig. 5D) and composition of this sample are similar to jotunites described from elsewhere in the Rogaland Anorthosite Province (Table 4). These jotunites (hypersthene monzodiorites rich in FeO and $TiO_2$ and relatively low in CaO) have been called "primitive jotunites" by Vander Auwera et al. (1998) because they are the least differentiated jotunites observed in Rogaland. Similar compositions are referred to as ferrodiorites or monzonorites by other authors (e.g. Mitchell et al., 1996) and are commonly associated with massif-type anorthosites. In the Rogaland Anorthosite Province, these rocks are found as dykes (Duchesne et al., 1974, 1985, 1989), as chilled margins of plutons such as Hidra and the Bjerkreim-Sokndal layered intrusion (Demaiffe and Hertogen, 1981; Duchesne and Hertogen, 1988; Robins et al., 1997), or as pillows in the Apophysis (Bolle, 1996). Sample 12.5V-6S (264) is considered to represent a melt composition.

Compositional arrays are distributed within triangles or display well-defined linear trends. Samples from LCZ and UCZ are well discriminated by the MgO content which is significantly higher in UCZ. This is a consequence of the presence of cumulus orthopyroxene and olivine in UCZ. Samples from LMZ and UMZ are relatively $TiO_2$-poor and are closer to the jotunite composition. These diagrams clearly demonstrate that compositional variations in the rocks essentially result from the occurrence of cumulus orthopyroxene and olivine in the UCZ (in addition to plagioclase and ilmenite in the LCZ), and from the content of a trapped jotunitic liquid component that is more abundant in the marginal zones.

## 7. Discussion

### 7.1. Sequence of crystallization: comparison with the Bjerkreim-Sokndal layered intrusion

The Bjerkreim-Sokndal layered intrusion crops out in the central part of the Rogaland Anorthosite Province (Michot, 1965; Duchesne, 1987; Wilson et al., 1996). The lower part of this intrusion consists of a 7000-m thick series of cumulates (the "Layered Series") and the upper part comprises acidic rocks, many of which are interpreted to represent liquid compositions (Duchesne and Wilmart, 1997). All units of the AMC series are developed: anorthosite, troctolite, leuconorite, norite, gabbronorite, jotunite, mangerite, quartz mangerite and charnockite. The parental magma of this intrusion has a jotunitic composition (Duchesne and Hertogen, 1988; Vander

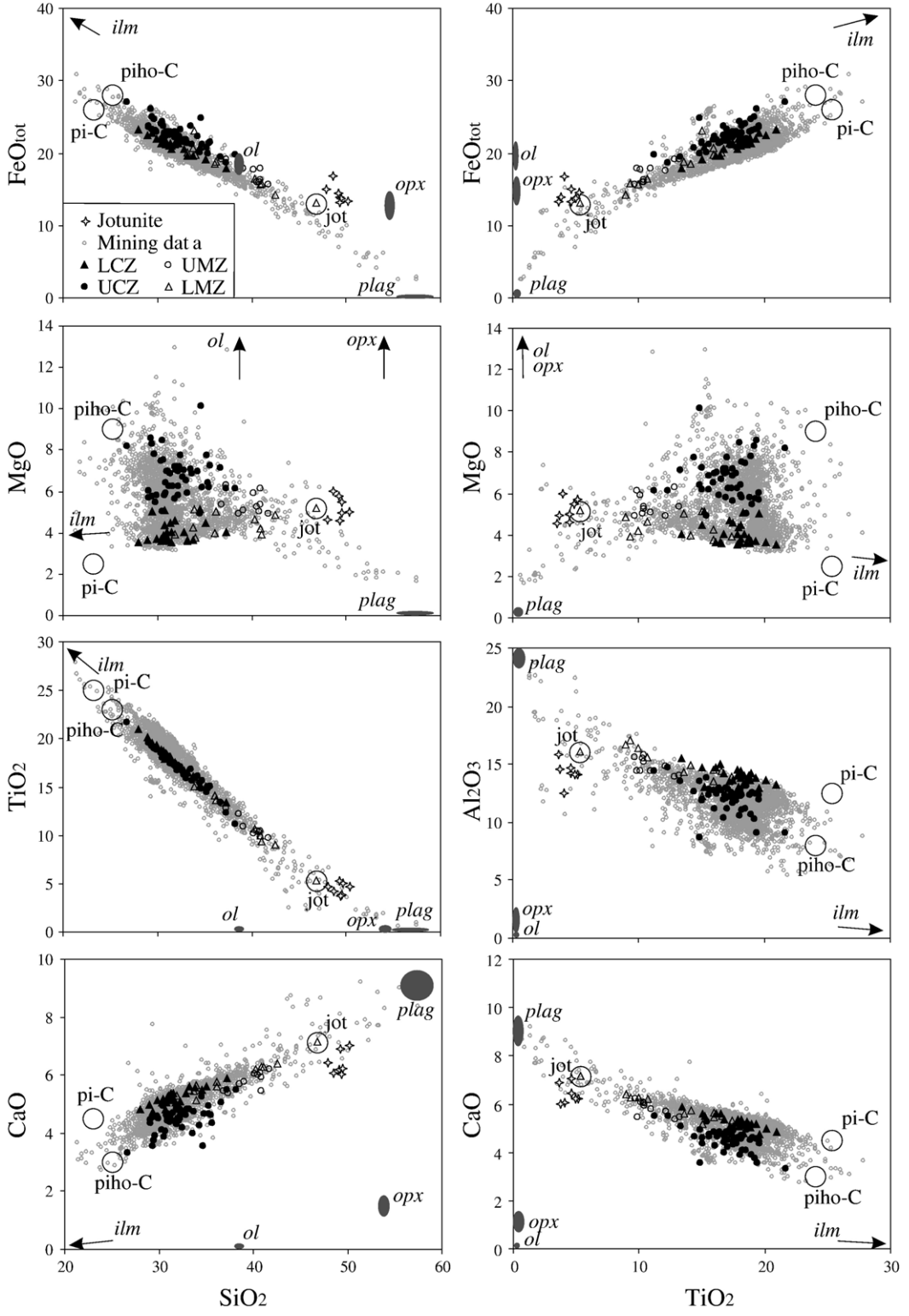


Fig. 9. Binary major elements variation diagrams of bulk cumulates from the Tellnes ilmenite deposit. The compositional ranges of cumulus minerals (plag=plagioclase, ilm=ilmenite, opx=orthopyroxene, ol=olivine) is represented by an elliptic area or indicated by an arrow (data from this study and Charlier et al., submitted for publication). The circled triangle is sample 12.5V-6S (264) (jot=jotunite). Other jotunites are from Table 4. Calculated adcumulate poles pi-C and piho-C are represented by a circle.

Table 4
Composition of the marginal sample from the Tellnes deposit compared to selected primitive jotunites from the Rogaland Anorthosite Province

| Sample | 12.5V-6S (264) | 80.12.3a | 80.12.4 | 80.12.1 | 91.14.1 | 70.20 | 200.2/2 | 72.34 | HLCA | TJ |
|---|---|---|---|---|---|---|---|---|---|---|
| Reference | This study | (4) | (3) | (3) | (5) | (1) | (2) | (1) | (6) | (6) |
| Locality | Tellnes | Tjörn-BKSK | BKSK | BKSK | BKSK | Hidra | Hidra | Hidra | | |
| $SiO_2$ | 46.84 | 49.39 | 49.27 | 49.57 | 50.38 | 48.00 | 48.68 | 49.53 | 50.0 | 49.5 |
| $TiO_2$ | 5.39 | 3.67 | 5.22 | 4.95 | 4.62 | 4.61 | 4.12 | 3.82 | 1.85 | 3.46 |
| $Al_2O_3$ | 16.10 | 15.81 | 14.00 | 14.11 | 14.65 | 14.20 | 12.40 | 14.50 | 17.5 | 16.0 |
| $FeO_{tot}$ | 13.07 | 13.11 | 14.31 | 13.55 | 13.20 | 14.90 | 16.62 | 13.68 | 10.8 | 13.1 |
| MnO | 0.14 | – | 0.15 | 0.14 | – | 0.18 | – | – | 0.15 | 0.13 |
| MgO | 5.18 | 4.54 | 5.71 | 5.46 | 4.98 | 4.60 | 5.96 | 4.90 | 6.67 | 4.54 |
| CaO | 7.15 | 6.87 | 6.18 | 6.21 | 7.01 | 6.41 | 6.04 | 6.00 | 8.78 | 6.82 |
| $Na_2O$ | 4.10 | 3.50 | 3.72 | 3.57 | 3.53 | 3.65 | 3.24 | 3.50 | 2.93 | 3.65 |
| $K_2O$ | 1.07 | 0.96 | 1.06 | 1.00 | 1.07 | 1.08 | 1.32 | 1.95 | 0.44 | 0.94 |
| $P_2O_5$ | 0.69 | 0.71 | 0.79 | 1.07 | 0.73 | 0.81 | 0.40 | 0.91 | 0.16 | 0.63 |
| Total | 99.73 | 98.56 | 100.41 | 99.63 | 100.17 | 98.44 | 98.78 | 98.79 | 99.3 | 98.8 |
| FeO[a] | 11.40 | 11.51 | 12.57 | 11.91 | 11.55 | 13.10 | 14.65 | 11.99 | 9.43 | 11.49 |
| $Fe_2O_3$[a] | 1.85 | 1.78 | 1.94 | 1.82 | 1.83 | 2.00 | 2.19 | 1.88 | 1.52 | 1.79 |
| mg# | 0.414 | 0.382 | 0.416 | 0.418 | 0.402 | 0.355 | 0.390 | 0.390 | 0.524 | 0.382 |
| NAb | 0.562 | 0.509 | 0.576 | 0.558 | 0.537 | 0.562 | 0.556 | 0.515 | 0.423 | 0.522 |
| NOr | 0.096 | 0.092 | 0.108 | 0.103 | 0.107 | 0.109 | 0.149 | 0.189 | 0.042 | 0.088 |

References: (1) Duchesne et al. (1974); (2) Demaiffe (1977); (3) Duchesne et al. (1989); (4) Duchesne and Hertogen (1988); (5) Vander Auwera et al. (1998); (6) Longhi et al. (1999).
[a] Calculated from Kress and Carmichael (1991) at FMQ and 1100 °C.

Auwera and Longhi, 1994; Robins et al., 1997). Detailed mapping and studies of mineral compositions (Michot, 1965; Duchesne, 1972; Nielsen and Wilson, 1991; Jensen et al., 1993; Nielsen et al., 1996; Jensen et al., 2003; Wilson and Overgaard, 2005) as well as experimental studies on the jotunitic parental magma (Vander Auwera and Longhi, 1994) have resulted in a detailed picture of the sequence of crystallization and magma chamber processes (Fig. 10). The Layered Series has been subdivided into 6 megacyclic units (MCU 0, IA, IB, II, III, and IV). Using the observed regressions in mineral compositions (Duchesne, 1972; Nielsen and Wilson, 1991; Jensen et al., 1993) and abrupt variations in isotopic ratios (Nielsen et al., 1996; Barling et al., 2000), it has been shown that each MCU resulted from the crystallization of a new magma influx that mixed with residual resident liquid. Isotopic variations also provide evidence for continuous assimilation of surrounding gneissic rocks (Tegner et al., 2005). The sequence of crystallization in the Layered Series (Wilson et al., 1996) is usually: plagioclase, ilmenite, (or plagioclase + olivine + ilmenite + magnetite), orthopyroxene, magnetite, clinopyroxene together with apatite, and then pigeonite (instead of orthopyroxene). Fayalitic olivine reappears in the Transition Zone, followed by mesoperthite in mangerites and finally quartz appears in quartz mangerites.

In the Tellnes deposit, the LCZ contains the most primitive cumulates and has plagioclase and ilmenite as cumulus minerals (pi-C). The LCZ would thus correspond to pi-C of zone a in Bjerkreim-Sokndal. This suggests that parental magmas to both intrusions were related as they had the same liquidus minerals. Cumulus orthopyroxene and olivine appear in the UCZ. This sequence of crystallization differs from the Bjerkreim-Sokndal layered intrusion where orthopyroxene does not seem to have been in equilibrium with olivine. As discussed below, these dissimilarities can be easily explained by small differences in parental magma compositions. Apatite and clinopyroxene do not appear as cumulus minerals in Tellnes. Duchesne and Charlier (2005) have shown that apatite appeared in Bjerkreim-Sokndal as a liquidus phase when the proportion of residual liquid (F) was about 0.6. This implies that the Tellnes deposit corresponds to the early stage of evolution of a jotunitic magma and is only the lower part of a larger intrusion. More evolved cumulates are not observed at the present level of exposure.

Toward the base of the Bjerkreim-Sokndal layered intrusion, a thick sequence of anorthositic cumulates (p-C) crystallized before pi-C, but such cumulates are absent in Tellnes. The origin of these anorthosites in MCU Ia and Ib has been discussed by Duchesne and Charlier (2005), who concluded that the parental magma of these units could have been different from the parental magma of MCU II to IV. Moreover, a higher $TiO_2$ content in the Tellnes parental magma could have been responsible for the earlier saturation in ilmenite (Toplis and Carroll, 1995), preventing the crystallization of a large volume of anorthosite.

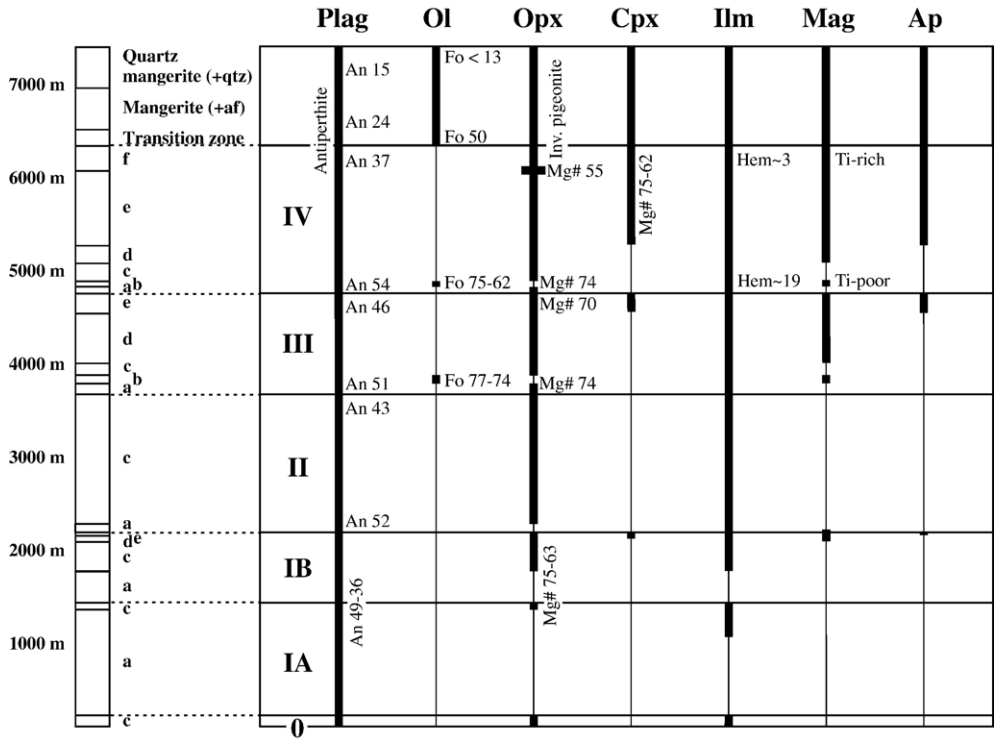


Fig. 10. Cumulate stratigraphy of the Bjerkreim-Sokndal layered intrusion as developed in the northern part of the intrusion along the axial trace of the syncline. The intrusion is subdivided into 6 megacyclic units (MCU 0, IA, IB, II, III and IV) in which compositional zones (a to f) are recognized. The compositional ranges of cumulus minerals are indicated (after Wilson et al., 1996). Cumulus assemblages following the nomenclature of Irvine (1982) in zones a to f : a = p(±i)-C; b = pimo-C; c = pih-C; d = pihm-C; e = pihmac-C; f = pih'mac-C. Mineral abbreviations: p = plagioclase; h = orthopyroxene; h′ = inverted pigeonite; o = olivine; i = ilmenite; m = magnetite; a = apatite; c = clinopyroxene; -C = cumulus.

Finally, the much higher proportion of ilmenite in Tellnes compared to Bjerkreim-Sokndal, where $TiO_2$ in bulk cumulates is around 3.7% on average (Duchesne and Charlier, 2005), necessitates either sorting and accumulation of ilmenite in the ore body or a significantly higher cotectic proportion of ilmenite in Tellnes due to different conditions of crystallization.

### *7.2. Sequence of crystallization: constraints from experimental studies and phase diagrams*

Experimental phase equilibrium data from 1 bar to 13 kb for magmas related to Proterozoic anorthosite have been presented by Fram and Longhi (1992), Vander Auwera and Longhi (1994), Vander Auwera et al. (1998), and Longhi et al. (1999). These phase diagrams for compositions TJ and HLCA, similar to the jotunite 12.5V-6S (264) (Table 4), enable us to assess crystallization conditions for the Tellnes ilmenite deposit. Indeed, sample 12.5V-6S (264), is interpreted to represent the trapped liquid component of the ore. Much evidence also points to this composition being close to the parental magma of the intrusion. In addition to compositional similarities with other primitive jotunites in Rogaland (Table 4), this fine-grained sample comes from the floor of the ore body, at the contact with the host anorthosite, exactly where the first injection of magma would have been quenched.

The progression of liquidus equilibria with pressure for the Tjörn composition (TJ, Table 4) calculated from the algorithms of Longhi (1991) is presented in Fig. 11A. The Opx-Ol liquidus boundary is a peritectic from 1 bar to 5 kb and becomes a cotectic at 7 kb due to the reduction of the stability field of olivine with pressure. A similar shift of the Opx-Ol liquidus boundary is observed in Fig. 11B for a different magma (HLCA, Table 4) at the same crystallization pressure of 5 kb. Higher *mg*-number and anorthite content of the normative feldspar have a similar effect on the position of the Opx-Ol liquidus boundary as increasing pressure (Longhi et al., 1999).

Discrepancies between the evolution in Bjerkreim-Sokndal (peritectic reaction of orthopyroxene and olivine) and in Tellnes (cotectic relation between orthopyroxene and olivine) can be explained by slightly different parental

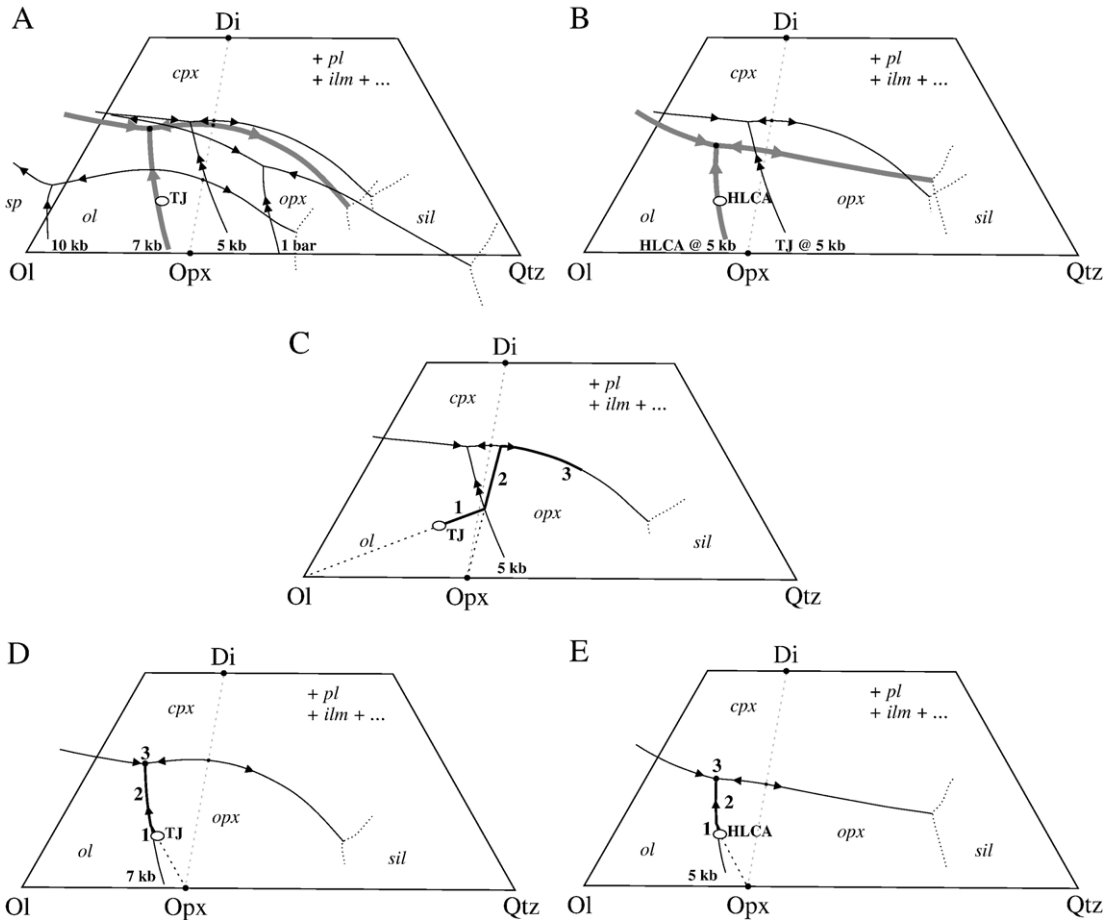


Fig. 11. Liquidus equilibria for magmas related to massif-type anorthosites projected from the Pl, Or and Ilm components onto the Ol–Qtz–Wo plane and calculated from the algorithms of Longhi (1991), modified after Longhi et al. (1999). (A) Progression of liquidus equilibria for TJ-like compositions (samples 80.12.3A) from 1 bar to 10 kbar. (B) Comparison between liquidus equilibria at 5 kb for HLCA and TJ compositions. (C) Fractional crystallization path for a TJ parental magma at 5 kb reproducing the crystallization sequence of Bjerkreim-Sokndal. (D) Fractional crystallization path for a TJ parental magma at 7 kb reproducing the crystallization sequence of Tellnes. (E) Fractional crystallization path for a HLCA parental magma at 5 kb reproducing the crystallization sequence of Tellnes. (Symbols: *pl* plagioclase, *ol* olivine, *opx* orthopyroxene, *cpx* clinopyroxene, *ilm* ilmenite, *gar* garnet, *sp* spinel, *sil* silica phase).

magma composition and/or by different pressure of emplacement. At the base of MCU III and IV of Bjerkreim-Sokndal (Fig. 10), the sequence of crystallization is plagioclase+olivine (+ilmenite,+magnetite), then plagioclase+orthopyroxene (+ilmenite, −magnetite) followed by plagioclase+orthopyroxene+clinopyroxene (+ilmenite,+magnetite,+apatite). This path is reproduced in Fig. 11C for fractional crystallization of the TJ parental magma at 5 kb. The sequence in Tellnes, where plagioclase (+ilmenite) is followed by plagioclase+orthopyroxene+olivine (+ilmenite) is displayed in Fig. 11D for fractional crystallization of the TJ parental magma at 7 kb, and in Fig. 11E for fractional crystallization of the HLCA parental magma at 5 kb. The simultaneous appearance of orthopyroxene and olivine in Tellnes result from the position of the melt on the Opx-Ol cotectic. The cotectic proportion of olivine to orthopyroxene is small which is consistent with the relatively low abundance of cumulus olivine in the upper part of Tellnes.

Whether the pressure of crystallization (5 vs. 7 kb; Fig. 11D) or the composition of the parental magma (Fig. 11E) is responsible for differences in the sequence of crystallization in the Bjerkreim-Sokndal layered intrusion compared to Tellnes may be assessed through the composition of liquidus phases in these two intrusions and in experimental products from the crystallization of TJ and HLCA. The TJ composition (at 5 kb) crystallizes plagioclase $An_{48}$ and olivine $Fo_{65}$ (Vander Auwera and Longhi, 1994). In Tellnes, the composition of liquidus plagioclase reaches $An_{56}$ (see below) and olivine in the

UCZ is around $Fo_{80}$ (Wilmart et al., 1989) and may reach $Fo_{84}$ (Charlier, unpublished data). These values are slightly more primitive than in the Bjerkreim-Sokndal layered intrusion were the most primitive compositions reported by Wilson et al. (1996) are $An_{54}$ and $Fo_{77}$. These values for Tellnes and Bjerkreim-Sokndal are closer to the composition of liquidus phases produced by the crystallization of the HLCA composition at 5 kb: $An_{64}$, $Fo_{76}$ (Fram and Longhi, 1992). In Tellnes, the higher Mg# of the melt when olivine appears in the UCZ probably results from the fractionation of plagioclase and ilmenite in the LCZ, both MgO-poor.

Consequently, we consider that the Tellnes parental magma was more primitive (higher Mg# and more anorthitic) than the TJ composition of Vander Auwera and Longhi (1994). These authors also concluded that TJ is too evolved to be parental to Bjerkreim-Sokndal. However, the Tellnes parental magma has jotunitic affinities and is probably close to the marginal sample 12.5V-6S (264) (Table 4) and slightly more primitive than the Bjerkreim-Sokndal parental magma. The more primitive character of the Tellnes parental magma is responsible for the cotectic orthopyroxene–olivine liquidus boundary in Tellnes. The pressure of crystallization is thus inferred to be the same for Tellnes and Bjerkreim-Sokndal, around 5 kb.

### *7.3. Compositional variations of plagioclase and whole-rocks*

A primary cryptic compositional variation of plagioclase due to fractional crystallization would be expected from LCZ to UCZ. Similarly, whole-rock compositions are believed to be influenced by the change in phase relations (+orthopyroxene and +olivine). Moreover, the presence of variable proportions of trapped liquid in Tellnes is shown by petrographical considerations and by the range of $P_2O_5$ contents. The crystallization of trapped liquid is known to potentially have a major influence on the compositions of cumulus minerals ("the trapped liquid shift" of Barnes, 1986) and of the bulk cumulates.

Plagioclase compositions plotted in various diagrams (Fig. 7) display well defined linear trends. This feature can be interpreted as the result of two-component mixing. One component, called the "primitive pole", has the approximate composition $An_{48}$, $Or_{3.0}$, 1170 ppm Sr and 150 ppm Ba. This represents plagioclase from the most primitive samples in the central zones which have low bulk $P_2O_5$ contents and are interpreted to be the closest preserved approximation to the primary cumulus plagioclase composition. The second component, called the "evolved pole", has the composition of plagioclase in 12.5V-6S (264): $An_{39.3}$, $Or_{7.1}$, 964 ppm Sr, and 355 ppm Ba. As mentioned above, sample 12.5V-6S (264) is interpreted as representing a liquid composition with jotunitic affinities. The range of plagioclase composition can thus be interpreted as a result of mixing between cumulus plagioclase ("primitive pole") and plagioclase that crystallized from the trapped liquid ("evolved pole"). All intermediate compositions are observed. Samples from the margins of the ore body are closer to the "evolved pole" whereas samples from the centre are nearer to the "primitive pole". This reflects a higher proportion of trapped liquid at the margins than in the centre of the body.

Triangular patterns of whole-rocks composition can be interpreted similarly but three poles are necessary (Fig. 9). The first pole has the composition of sample 12.5V-6S (264), and represents the trapped liquid component of the bulk cumulates. The second pole is represented by a $TiO_2$-rich cumulate, close to that of LCZ. This pole thus belong to a group of rocks which have plagioclase and ilmenite as cumulus minerals (pi-C), with zero trapped liquid. The third pole is MgO-rich and is close to cumulates of the UCZ where plagioclase, ilmenite, orthopyroxene and olivine are cumulus minerals (piho-C) and the trapped liquid fraction is zero. Linear trends simply result from the alignment of the three poles (e.g. $TiO_2$–$SiO_2$, Fig. 9). The compositions of plagioclase in LCZ and in UCZ are not significantly different (Fig. 6) and plot on a single linear trend (Fig. 7) because the trapped liquid shift overprints the effects of fractional crystallization. Samples from the UCZ do not display a simple linear trend in bulk cumulate compositions between a pure adcumulate and the jotunite composition. This results from the increasing proportion of orthopyroxene upwards through the UCZ (see Table 1).

The composition of these cumulate poles and their relative proportions of cumulus phases are calculated by subtracting the effect of the trapped liquid from the bulk cumulate compositions. This can be done by assuming that a pure adcumulate does not contain any $P_2O_5$. The intercept for 0% $P_2O_5$ gives the composition of the pure adcumulate. This is illustrated on Fig. 12A for MgO. The composition and the average modal proportions of cumulus minerals for the two types of cumulates (pi-C and piho-C) is given in Table 5. For pi-C, the linear trend between the adcumulate and the trapped liquid compositions (Fig. 12A) is well-defined which means that the relative proportion of cumulus plagioclase and ilmenite (p: 44 wt.%; i: 56 wt.%) remains constant. The variability of plagioclase/ilmenite proportions in bulk cumulates results from variable contents of trapped liquid, which has

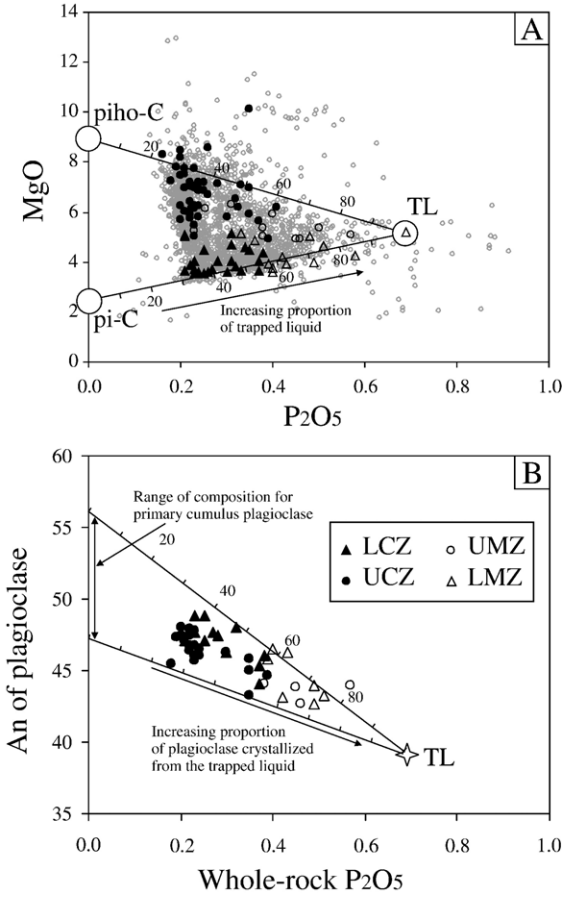


Fig. 12. (A) MgO vs. $P_2O_5$ for bulk cumulates from the Tellnes ilmenite deposit with the calculated proportion of trapped liquid assuming 0% liquid component for 0% $P_2O_5$ and 100% in the jotunite representing the trapped liquid composition (TL) (Same legend as Fig. 10). (B) An content of plagioclase vs. $P_2O_5$ of the bulk cumulates of the Tellnes ilmenite deposit with the calculated proportion of trapped liquid assuming 0% liquid component for 0% $P_2O_5$ and 100% in the plagioclase from the jotunite (TL).

a higher plagioclase/ilmenite proportion than the cumulus assemblage. The trend is more variable for piho-C, particularly for MgO (Fig. 9). This results from the continuous increase in the modal proportion of orthopyroxene towards the top of the UCZ. In this case, an increase in the rate of orthopyroxene accumulation in the course of crystallization is suspected. Two different proportions have therefore been calculated. The first one, piho-C (1) (p: 37 wt.%; i: 52 wt.%; h+o: 11 wt.%) represents the proportions of cumulus phases at the appearance of cumulus orthopyroxene and olivine, and the second one, piho-C (2) (p: 30 wt.%; i: 49 wt.%; h+o: 21 wt.%), are the proportions for the most evolved cumulates observed in Tellnes. There is a continuous gradation in modal proportions from the first to the second.

### *7.4. Abundance, role and compositional variation of trapped liquid*

The trapped liquid proportion can be quantitatively estimated with the following method. As apatite is interstitial and the $P_2O_5$ content of the cumulus minerals (plagioclase, ilmenite, orthopyroxene and olivine) can be neglected, we can assume that all $P_2O_5$ is present in the trapped liquid. Knowing that sample 12.5V-6S (264), which is considered to represent the composition of the trapped liquid, has 0.69% $P_2O_5$, it is possible to calculate the proportion of trapped liquid in each sample. In bulk cumulates, $P_2O_5$ ranges from 0.16 to 0.58%, corresponding to a proportion of trapped liquid between 23 and 83%. Graphically, the amount of trapped liquid can illustrated in the diagram MgO–$P_2O_5$ (Fig. 12A). The higher proportion of trapped liquid in samples from marginal zones results from a higher rate of cooling near the margins with the host anorthosite, preventing the migration of trapped liquid and resulting in a chilled margin. The proportion of trapped liquid can also be calculated by comparing plagioclase compositions with the $P_2O_5$ content of the bulk cumulate (Fig. 12B). In this case, the presence of trapped liquid decreases the An content of the bulk plagioclase composition. The unmodified composition of cumulus plagioclase as obtained for 0% trapped liquid (0% $P_2O_5$) varies between $An_{47}$ and $An_{56}$. This range of plagioclase compositions is close to the data for the most primitive cumulates of the Bjerkreim-Sokndal layered intrusion (Fig. 10), but

Table 5
Composition and mineral proportions of theoretical adcumulate poles of the Tellnes ilmenite deposit

| | Pole pi-C | Pole piho-C (1) | Pole piho-C (2) |
|---|---|---|---|
| *Major elements composition of bulk adcumulates (wt.%)* | | | |
| $SiO_2$ | 23.0 | 25.0 | 25.0 |
| $TiO_2$ | 25.3 | 24.5 | 23.0 |
| $Al_2O_3$ | 12.5 | 10.0 | 8.0 |
| $FeO_{tot}$ | 26.0 | 27.0 | 28.0 |
| MnO | 0.12 | 0.13 | 0.15 |
| MgO | 2.5 | 5.5 | 9.0 |
| CaO | 4.5 | 3.5 | 3.0 |
| $Na_2O$ | 2.5 | 2.2 | 2.0 |
| $K_2O$ | 0.2 | 0.2 | 0.2 |
| $P_2O_5$ | 0.0 | 0.0 | 0.0 |
| Total | 96.62 | 98.03 | 98.35 |
| *Proportions of cumulus minerals (wt.%)*[a] | | | |
| Plag | 46 | 37 | 30 |
| Ilm | 54 | 52 | 49 |
| Opx+Ol | 0 | 11 | 21 |

[a] Calculated with $Al_2O_3$ in plagioclase, $TiO_2$ in ilmenite; Opx+Ol by difference.

slightly more calcic. This justifies the interpretation from phase diagrams that the Tellnes parental magma was slightly more primitive compared to the Bjerkreim-Sokndal parental magma.

The spatial distribution of the trapped liquid fraction is shown in Fig. 13 for section 1600. This trapped liquid fraction decreases continuously from the margin to the centre of the ore body. At >100 m from the contact, the trapped liquid fraction seems to stabilize around 30%. Following the terminology of Irvine (1982), cumulates from Tellnes are mainly orthocumulates (the trapped liquid fraction is between 25 and 50%). This is surprising in view of the depth of emplacement (5 kb) and presumably a relatively slow rate of crystallization.

Calculations of the trapped liquid fraction have been done under the assumption that the trapped liquid maintains the same composition. However, fractional crystallization causes $P_2O_5$ enrichment in the residual liquid until cumulus apatite appears. So, in more evolved cumulates, and particularly in piho-C, the $P_2O_5$ content of the magma was higher than in the magma crystallizing pi-C cumulates. The calculated proportion of trapped liquid is, therefore, increasingly overestimated upwards. To estimate the maximum error, we can consider that the most evolved cumulate at the top of section 1600 (Fig. 13) crystallized when the fraction of residual liquid was 0.6, which is the maximum on the arrival of cumulus apatite by analogy with Bjerkreim-Sokndal (Duchesne and Charlier, 2005). For incompatible elements, the liquid composition ($C_{liq}$) follows the simplified Rayleigh equation $C_{liq}=C_0/F=1.15$ (for $F=0.6$) where $C_0$ is the $P_2O_5$ content (=0.69%) in the parental magma. The trapped liquid fraction in cumulates from the upper part of section 1600 ($P_2O_5=\sim 0.22\%$) is thus 19% and not around 32%. The calculated trapped liquid fractions with this correction are shown in Fig. 13.

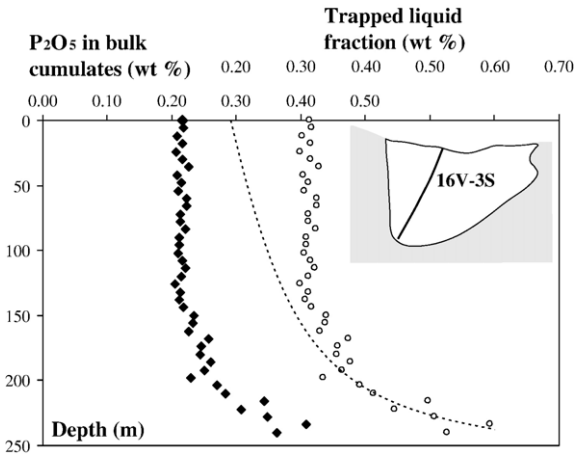


Fig. 13. $P_2O_5$ in bulk cumulates and trapped liquid fraction ($P_2O_5$ in bulk cumulate/$P_2O_5$ in the parental magma) as a function of the depth (m) in drill core 16V-3S. The dotted line represents the trapped liquid fraction corrected for the $P_2O_5$ increase of the trapped liquid due to fractional crystallization of the parental magma. Each mining data corresponds to 6 m of the drill core (number of sample=41).

### 7.5. Cotectic proportions or sorted cumulates?

One of the main questions concerning the formation of the ore is how ilmenite was concentrated and why the proportion of ilmenite to plagioclase is so high. Mineral sorting is a process that may be responsible for compositional variations. Therefore it is important to determine if the relative proportions of cumulus minerals represent cotectic proportions or not, i.e. whether the cumulates have been sorted. In Tellnes, and particularly in the LCZ, variations in whole-rock compositions (Fig. 9) cannot be explained by a variable content of one of the cumulus minerals because trends do not always point towards either plagioclase or ilmenite. Moreover, whole-rock compositions are always restricted to well-defined triangles in different diagrams, and the most important cause of compositional variability seems to be the proportion of trapped liquid. However, as previously mentioned, the proportion of ilmenite in Tellnes is higher compared to its proportion in Bjerkreim-Sokndal. Moreover, even if the experimentally estimated cotectic proportions of Toplis and Carroll (1995) vary with temperature and oxygen fugacity, the ilmenite abundance is never higher than 6.5 vol.%. This points to significant ilmenite accumulation in Tellnes where the ilmenite proportion can reach ~40 vol.% in the LCZ. This issue is further discussed by Charlier et al. (submitted for publication) who have calculated that the cotectic proportion of ilmenite in Tellnes is close to 17 wt.% by modelling ilmenite composition with the Rayleigh equation.

The ore body represents the lower part of a larger intrusion. This must be borne in mind when considering possible magma chamber processes. The unexposed upper part of the ore body may contain a large amount of plagioclase which could have accumulated due to its buoyancy in the relatively dense melt (~2.75, Vander Auwera et al., in press). However, because the cumulus plagioclase/ilmenite proportions remain globally constant, the amount of plagioclase removed by flotation must have been kept constant throughout the course of crystallization of the exposed part of Tellnes. In other words, the rate of ilmenite accumulation was consistently higher than the rate of plagioclase accumulation.

### 7.6. Emplacement mechanism of the Tellnes ilmenite deposit

Wilmart et al. (1989) proposed that the ilmenite-rich norite was injected as a crystal-mush lubricated by 3 to 10% trapped liquid. This mechanism of emplacement was later supported by magnetic and petrofabric evidence (Diot et al., 2003). Our new data reveal more complex relationships in major element variation diagrams than the simple mixing line observed by Wilmart et al. (1989), and exclude an emplacement mechanism involving the injection of a crystal-mush. We have shown that the leucocratic pole in variation diagrams is not an anorthositic cumulate as proposed by Wilmart et al. (1989), but represents the trapped liquid component. The stratigraphic succession of two types of cumulate, pi-C followed by piho-C, can hardly be explained by the injection of a mush but favours in situ crystallization within the Tellnes magma chamber.

Several points can be discussed concerning the orientation of the ore based on magnetic and petrofabric evidence (Diot et al., 2003). These authors concluded that Tellnes was injected into a zone of weakness in the Åna-Sira anorthosite, under brittle conditions. However, they describe irregular, sinuous magmatic contacts on the northern flank, concordant with the host anorthosite. This favours an emplacement into ductile anorthosite, corroborated by the irregular and sinuous network of small dykes in the south-eastern part. Considering the microtextures and the criteria proposed by Nicolas (1987) and Paterson et al. (1989) to distinguish magmatic from solid-state deformation, plagioclase and orthopyroxene show evidence of plastic strain in crystals resulting from high-T solid-state deformation (bending, undulatory extinction, kinking and partial recrystallization). These deformation textures could not have been contemporaneous with the emplacement because there is no relation between the degree of deformation and recrystallization of a sample and its trapped liquid fraction (TLF). Samples with >40% of TLF, much above the critical melt fraction when no deformation can affect solids (Van der Molen and Paterson, 1979), can display a higher deformation than samples with lower TLF. These new considerations imply that the mineral lineation must be explained by other mechanisms than by flow of a crystal mush.

We propose that the ilmenite-rich norite crystallized in situ in a sill-shaped magma chamber with a floor dipping to the south-east, injected into the Åna-Sira anorthosite under ductile conditions. Solid-state deformation of the sill was subsequently produced by subsidence. The direction of the Tellnes subsidence is relative to the host anorthosite because the movement can either have been produced by gravity-induced sinking of the high-density Tellnes intrusion into the low-density Åna-Sira anorthosite or/and by the rising of the anorthosite diapir. Actually, this last movement is probably responsible for the rotation of the ore body to the NE because the centre of the diapir was situated SW to the ore body. This explains the vertical SW flank and why the Lower Central Zone is stratigraphically higher on the SW flank compared to the NE flank (Fig. 6).

This subsidence is responsible for deformation of the minerals and the present shape of the ore body, producing the magnetic lineation and the 18° SE plunge of the floor. This is similar to the mechanism described by Paludan et al. (1994) and Bolle et al. (2002) to explain deformation of the Bjerkreim-Sokndal layered intrusion. Our model can be summarized in three successive stages. First, a jotunitic magma was emplaced in a sill-shaped magma chamber. As the parental magma cooled, pi-C accumulated at the bottom of the chamber, followed by piho-C, with a higher rate of ilmenite accumulation compared to plagioclase, probably buoyant in the dense jotunitic melt. The high thermal gradient at the margins induced formation of rapidly-cooled margins (LMZ and UMZ). Even in the centre of the ore body, large amounts of liquid (20–30%) became trapped in the cumulates. The exposed portion of the deposit represents the lower part of a larger magma chamber. At the present erosion level, no evolved cumulates or other rocks that crystallised from residual liquid are preserved. Finally, the cumulates were deformed by gravity-induced subsidence and by anorthosite diapirism, producing the present asymmetric trough-shape cross section of the ore body. This deformation is responsible for the solid-state recrystallization of minerals and for the present magnetic fabric orientation.

### 7.7. The origin of Fe–Ti ores: a synthesis

Several mechanisms have been suggested for the genesis of ilmenite deposits associated with massif-type anorthosites. Philpotts (1967) and Kolker (1982) argued for immiscible Fe–Ti–P-rich melts. Unrealistically high temperatures for the ilmenite–apatite melts (~1400 °C) and experimental studies by Lindsley (2003) do not favour immiscibility. Furthermore, constant proportions of mafic minerals in cumulates from the Bjerkreim-Sokndal layered intrusion (Duchesne and Charlier, 2005) preclude the formation of an immiscible Fe–Ti rich liquid during the course of crystallization. The interstitial habit of ilmenite and the existence of ilmenite-rich veins in anorthosite are the result of subsolidus grain boundary modifications and solid-state deformation rather than liquid immiscibility (Duchesne, 1996).

Robinson et al. (2003) suggested that magma mixing was responsible for the high proportion of ilmenite in Tellnes. However, as illustrated throughout this work, ilmenite is never the only liquidus mineral but crystallized either together with plagioclase or with plagioclase, orthopyroxene and olivine. Moreover, the hypothetical curved ilmenite–plagioclase cotectic invoked by these authors, similar to the curved chromite–olivine cotectic (Irvine, 1977), has no experimental support. Magma mixing in chambers emplaced in the continental crust is typically accompanied by systematic variations in mineral compositions and isotopic ratios. The very restricted range of variation of Sr isotopes in the Tellnes deposit (Table 2) does not favour such mixing as a mechanism for ilmenite enrichment.

Finally, the Ti budget is not problematic at all. The parental magma of Tellnes (sample 12.5V-6S, 264) and other related melts in the Rogaland Anorthosite Province have more than 4% $TiO_2$ (Table 4). This is not a feature that is restricted to Rogaland because $TiO_2$-rich liquids have been described in other anorthositic complexes (e.g. Mitchell et al., 1996), and even in modern lavas of continental tholeiitic suites such as Craters of the Moon or Snake River Plain (Nekvasil et al., 2000).

It emerges that the only plausible mechanism for the formation of ilmenite deposits is simply fractional crystallisation. Parental magmas are Ti-rich and crystallize ilmenite as an early liquidus mineral. Parameters controlling the sequence of crystallization (e.g. ilmenite before or after orthopyroxene) and the exact cotectic proportions are presently not constrained by experimental studies. Further studies on the role of magma composition, pressure and $fO_2$ are needed. Sorting of ilmenite due to a higher rate of accumulation compared to plagioclase is easily explained by different densities (2.7 vs. 4.8 g $cm^{-3}$). Under appropriate conditions, we suggest that this mechanism can result in a pure ilmenite body, such as the Lac Tio deposit. This would preferentially happen in a slowly cooling magma chamber rather than in a small, rapidly-cooled body of magma such as at Tellnes.

## 8. Conclusions

The Tellnes ilmenite deposit is not an homogeneous ore body. Study of three N–S cross-sections reveals systematic variations in the cumulus assemblage. In the lower part (LCZ), plagioclase and ilmenite are the only cumulus minerals, followed by the appearance of orthopyroxene and olivine in the upper part (UCZ). Marginal Zones (UMZ and LMZ) are characterized by high plagioclase and apatite contents and lower proportions of ilmenite. Phase diagrams for magmas related to massif-type anorthosites reproduce the sequence of crystallization observed in Tellnes for fractional crystallization of a primitive jotunite at 5 kb. The composition of the parental liquid for the ore body, identified by the occurrence at the base of the intrusion of a fine-grained rock at the contact with the host anorthosite, has a jotunitic composition slightly more primitive (more anorthitic and higher Mg #) than that of the Bjerkreim-Sokndal layered intrusion. Exposed cumulates in Tellnes correspond to the first stage of evolution of a jotunitic magma. The ore body is thus interpreted as the lower part of a larger intrusion.

The proportion of trapped liquid is the main cause of variability of the compositions of plagioclase and bulk cumulates. Estimation of the trapped liquid proportion reveals that it varies from about 20 to 80%. This proportion is greater at the margins where the cooling rate was higher, and it continuously decreases towards the centre of the ore body. Constant Sr isotopes ratios preclude significant contamination and give no evidence of magma mixing. The proportion of ilmenite, up to 50 wt.% in the LCZ, is not cotectic. A higher rate of ilmenite accumulation, due to plagioclase buoyancy in a dense jotunitic melt is invoked. The orientation of the minerals and the present trough-shape of the ore body were acquired during subsidence of the dense ore body into the Åna-Sira anorthosite and by up-doming of the anorthosite.

Based on general considerations of the genesis of ilmenite ores in massif-type anorthosites, it seems that fractional crystallization of a $TiO_2$-rich magma with ilmenite as an early liquidus minerals is the most plausible origin.

## Acknowledgements

This work was funded by the Belgian Fund for Joint Research and the Fund for Research in Industry and Agriculture. Fieldwork was partly supported by the Fourmarier Foundation. TITANIA A/S is gratefully acknowledged for providing access to chemical data on the Tellnes deposit and for supporting the cost of new analyses. Kari Berge and Ragnar Hagen are thanked for their continuous interest and encouragement. We also acknowledge Kåre Kullerud for sharing unpublished microprobe data as well as Olivier Bolle and Rais Latypov for their useful remarks. Comments from Judith Hannah and Richard Wilson have greatly improved an earlier version of the manuscript. This paper has benefited from constructive reviews by Sarah-Jane Barnes and Brian Robins. **[RLR]**

## References


Ashwal, L., 1993. Anorthosites. Springer, Heidelberg.

Barling, J., Weis, D., Demaiffe, D., 2000. A Sr-, Nd- and Pb-isotopic investigation of the transition between two megacyclic units of the Bjerkreim-Sokndal layered intrusion, south Norway. Chemical Geology 165, 47–65.

Barnes, S.J., 1986. The effect of trapped liquid crystallization on cumulus mineral compositions in layered intrusions. Contributions to Mineralogy and Petrology 93, 524–531.

Barnichon, J.-D., Havenith, H., Hoffer, B., Charlier, R., Jongmans, D., Duchesne, J.C., 1999. The deformation of the Egersund Ogna massif, south Norway: finite element modelling of diapirism. Tectonophysics 303, 109–130.

Bédard, J.H., 2001. Parental magmas of the Nain plutonic suite anorthosites and mafic cumulates: a trace element modelling approach. Contributions to Mineralogy and Petrology 141, 747–771.

Bindeman, I.N., Davis, A.M., Drake, M.J., 1998. Ion microprobe study of plagioclase–basalt partition experiments at natural concentration levels of trace elements. Geochimica et Cosmochimica Acta 62, 1175–1193.

Bingen, B., Stein, H.J., 2003. Molybdenite Re–Os dating of biotite dehydration melting in the Rogaland high-temperature granulites, S. Norway. Earth and Planetary Science Letters 208, 181–195.

Bingen, B., van Breemen, O., 1998. U–Pb monazite ages in amphibolite- to granulite-facies orthogneiss reflect hydrous mineral breakdown reactions: Sveconorwegian Province of SW Norway. Contributions to Mineralogy and Petrology 132, 336–353.

Bingen, B., Demaiffe, D., van Breemen, O., 1998. The 616-My-old Egersund basaltic dike swarm, SW Norway, and the Late Proterozoic opening of the Iapetus Ocean. The Journal of Geology 106, 565–574.

Bolle, O., 1996. Mélanges magmatiques et tectonique gravitaire dans l'Apophyse de l'intrusion de Bjerkreim-Sokndal (Rogaland, Norvège). Pétrologie, géochimie et fabrique magnétique. Ph.D. dissertation, Université de Liège.

Bolle, O., Trindade, R.I.F., Bouchez, J.L., Duchesne, J.C., 2002. Imaging downward granitic magma transport in the Rogaland Igneous Complex, SW Norway. Terra Nova 14, 87–92.

Bolle, O., Demaiffe, D., Duchesne, J.C., 2003. Petrogenesis of jotunitic and acidic members of an AMC suite (Rogaland Anorthosite Province, SW Norway): a Sr and Nd isotopic assessment. Precambrian Research 124, 185–214.

Bologne, G., Duchesne, J.C., 1991. Analyse des roches silicatées par spectrométrie de fluorescence X: précision et exactitude. Professional Papers - Geological Survey of Belgium 249, 1–11.

Charlier, B., Skår, Ø., Korneliussen, A., Duchesne, J.C., Vander Auwera, J., submitted for publication. Major and trace element composition of ilmenite in the Tellnes Fe–Ti deposit: fractional crystallization model and postcumulus evolution.

Demaiffe, D., 1977. Les massifs satellites anorthosito-leuconoritiques d'Hidra et de Garsaknatt: leur signification pétrogénétique. Annales de la Société Géologique de Belgique 100, 167–174.

Demaiffe, D., Hertogen, J., 1981. Rare earth element geochemistry and strontium isotopic composition of a massif-type anorthositic–charnockitic body: the Hidra Massif (Rogaland, SW Norway). Geochimica et Cosmochimica Acta 45, 1545–1561.

Diot, H., Bolle, O., Lambert, J.-M., Launeau, P., Duchesne, J.C., 2003. The Tellnes ilmenite deposit (Rogaland, south Norway): magnetic and petrofabric evidence for emplacement of a Ti-enriched noritic crystal mush in a fracture zone. Journal of Structural Geology 25, 481–501.

Duchesne, J.C., 1972. Iron–titanium oxide minerals in the Bjerkrem-Sogndal Massif, south-western Norway. Journal of Petrology 13, 57–81.

Duchesne, J., 1987. The Bjerkreim-Sokndal Massif. In: Maijer, C., Padget, P. (Eds.), The Geology of the Southernmost Norway. Norske Geologiske Undersøkelse Special Publication, pp. 56–59.

Duchesne, J., 1996. Liquid ilmenite or liquids ilmenite: a comment on the nature of ilmenite vein deposits. In: Demaiffe, D. (Ed.), Petrology and Geochemistry of Magmatic Suites of Rocks in the Continental and Oceanic Crusts. A Volume Dedicated to Professor Jean Michot. Université Libre de Bruxelles: Royal Museum for Central Africa, Tervuren, pp. 73–82.

Duchesne, J.C., 1999. Fe–Ti deposits in Rogaland anorthosites (south Norway): geochemical characteristics and problems of interpretation. Mineralium Deposita 34, 182–198.

Duchesne, J., 2001. The Rogaland Intrusive Massifs, an Excursion Guide. NGU report 2001. Geological Survey of Norway 29.

Duchesne, J.C., Charlier, B., 2005. Geochemistry of cumulates from the Bjerkreim-Sokndal layered intrusion (S. Norway). Part I: constraints from major elements on the mechanism of cumulate formation and on the liquid line of descent. Lithos 83, 229–254.

Duchesne, J.C., Hertogen, J., 1988. Le magma parental du lopolithe de Bjerkreim-Sokndal (Norvège méridionale). Comptes Rendus de l'Académie des Sciences de Paris 306, 45–48.

Duchesne, J.C., Wilmart, E., 1997. Igneous charnockites and related rocks from the Bjerkreim-Sokndal layered intrusion (southwest Norway): a jotunite (hypersthene monzodiorite)-derived A-type granitoid suite. Journal of Petrology 38, 337–369.

Duchesne, J.C., Roelandts, I., Demaiffe, D., Hertogen, J., Gijbels, R., De Winter, J., 1974. Rare-earth data on monzonoritic rocks related to anorthosites and their bearing on the nature of the parental magma of the anorthositic series. Earth and Planetary Science Letters 24, 325–335.

Duchesne, J.C., Roelandts, I., Demaiffe, D., Weis, D., 1985. Petrogenesis of monzonoritic dykes in the Egersund-Ogna anorthosite (Rogaland, S.W. Norway): trace elements and isotopic (Sr–Pb) constraints. Contributions to Mineralogy and Petrology 90, 214–225.

Duchesne, J.C., Wilmart, E., Demaiffe, D., Hertogen, J., 1989. Monzonorites from Rogaland (southwest Norway): a series of rocks coeval but not comagmatic with massif-type anorthosites. Precambrian Research 45, 111–128.

Duchesne, J.C., Liégeois, J.P., Vander Auwera, J., Longhi, J., 1999. The crustal tongue melting model and the origin of massive anorthosites. Terra Nova 11, 100–105.

Emslie, R.F., Hamilton, M.A., Thériault, R.J., 1994. Petrogenesis of a Mid-Proterozoic anorthosite–mangerite–charnockite–granite (AMCG) complex: isotopic and chemical evidence from the Nain plutonic suite. Journal of Geology 102, 539–558.

Fram, M., Longhi, J., 1992. Phase equilibria of dikes associated with Proterozoic anorthosite complexes. American Mineralogist 77, 605–616.

Gierth, E., 1970. Die Ilmenitlagerstätte Tellnes (Süd-Norwegen). Ph.D. dissertation, T.U. Clausthal.

Gierth, E., 1983. Types and trace elements of titanium ores in the Tellnes area south-Rogaland. Monograph Series on Mineral Deposits 22, 47–57.

Gierth, E., Krause, H., 1973. Die ilmenitlagerstätte Tellnes (Süd-Norwegen). Norsk Geologisk Tidsskrift 53, 359–402.

Gierth, E., Krause, H., 1974. Contribution to the mineralogy of Norway, No. 57: Baddeleyit von Tellnes. Norsk Geologisk Tidsskrift 54, 193–197.

Gierth, E., Krause, H., Schott, W., 1982. Paragenesen und gefüge des hydrothermalen nachhalls in südwestnorwegischen titaneisenerzen. Erzmetall 35, 441–446.

Grove, T.L., Baker, M.B., Kinzler, R.J., 1981. Coupled CaAl–NaSi diffusion in plagioclase feldspar: experiments and application to cooling rate speedometry. Geochimica et Cosmochimica Acta 58, 2113–2121.

Hunter, R.H., 1996. Texture development in cumulate rocks. In: Cawthorn, R.G. (Ed.), Layered Intrusions. Elsevier, Amsterdam, pp. 77–101.

Irvine, T.N., 1977. Origin of chromitite layers in the Muskox intrusion and other stratiform intrusions: a new interpretation. Geology 5, 273–277.

Irvine, T.N., 1982. Terminology for layered intrusions. Journal of Petrology 23, 127–162.

Jensen, J.C., Nielsen, F.M., Duchesne, J.C., Demaiffe, D., Wilson, J. R., 1993. Magma influx and mixing in the Bjerkreim-Sokndal layered intrusion, south Norway: evidence from the boundary between two megacyclic units at Storeknuten. Lithos 29, 311–325.

Jensen, K.K., Wilson, J.R., Robins, B., Chiodoni, F., 2003. A sulphide-bearing orthopyroxenite layer in the Bjerkreim-Sokndal Intrusion, Norway: implications for processes during magma-chamber replenishment. Lithos 67, 15–37.

Kolker, A., 1982. Mineralogy and geochemistry of Fe–Ti oxide and apatite (nelsonite) deposits and evaluation of the liquid immiscibility hypothesis. Economic Geology 77, 1146–1148.

Krause, H., Pape, H., 1977. Untersuchungen zum geologischen und petrographischen aufbau des Storgangen-ilmeniterzkörpers und seiner nebengesteinseinheiten (Süd-Norwegen). Norsk Geologisk Tidsskrift 57, 263–284.

Krause, H., Zeino-Mahmalat, R., 1970. Untersuchungen an erz und nebengestein der grube Blåfjell in SW-Norwegen. Norsk Geologisk Tidsskrift 50, 45–88.

Krause, H., Gierth, E., Schott, W., 1985. Fe–Ti deposits in the south Rogaland igneous complex, especially in the anorthosite-massif of Åna-Sira. Norges Geologiske Undersøkelese 402, 25–37.

Kress, V.C., Carmichael, I.S.E., 1991. The compressibility of silicate liquids containing Fe2O3 and the effect of composition, temperature, oxygen fugacity and pressure on their redox states. Contributions to Mineralogy and Petrology 108, 82–92.

Kullerud, K., 2003. Geochemistry and mineralogy of the Tellnes ore body. Norges Geologiske Undersøkelse Special Publication 9, 70–71.

Lafrance, B., John, B.E., Scoates, J.S., 1996. Syn-emplacement recrystallization and deformation microstructures in the Poe Mountain anorthosite, Wyoming. Contributions to Mineralogy and Petrology 122, 431–440.

Lindsley, D.H., 2003. Do Fe–Ti oxide magmas exist? Geology: yes; experiments: no! Norges Geologiske Undersøkelse Special Publication 9, 34–35.

Longhi, J., 1991. Comparative liquidus equilibria of hypersthene-normative basalts at low pressure. American Mineralogist 76, 785–800.

Longhi, J., 2005. A mantle or mafic crustal source for Proterozoic anorthosites? Lithos 83, 183–198.

Longhi, J., Vander Auwera, J., Fram, M., Monthieth, J.N., 1993. Pressure effects, kinetics and rheology of anorthositic and related magmas. American Mineralogist 78, 1016–1030.

Longhi, J., Vander Auwera, J., Fram, M.S., Duchesne, J.C., 1999. Some phase equilibrium constraints on the origin of Proterozoic (massif) anorthosites and related rocks. Journal of Petrology 40, 339–362.

Maijer, C., 1987. The metamorphic envelope of the Rogaland intrusive complex. In: Maijer, C., Padget, P. (Eds.), The Geology of the Southernmost Norway. Norske Geologiske Undersøkelse Special Publication, pp. 68–72.

Michot, P., 1965. Le magma plagioclasique. Geologische Rundschau 54, 956–976.

Mitchell, J.N., Scoates, J.S., Frost, C.D., Kolker, A., 1996. The geochemical evolution of anorthosite residual magmas in the Laramie Anorthosite Complex, Wyoming. Journal of Petrology 37, 637–660.

Möller, A., O'Brien, P.J., Kennedy, A., Kröner, A., 2002. Polyphase zircon in ultrahigh-temperature granulite (Rogaland, SW Norway): constraints for Pb diffusion in zircon. Journal of Metamorphic Geology 20, 727–740.

Nekvasil, H., Simon, A., Lindsley, D.H., 2000. Crystal fractionation and the evolution of intra-plate hy-normative igneous suites: insight from their feldspars. Journal of Petrology 41, 1743–1757.

Nicolas, A., 1987. Principles of Rock Deformation. D. Reidel, Dordrecht.

Nielsen, F.M., Wilson, J.R., 1991. Crystallization processes in the Bjerkreim-Sokndal layered intrusion, south Norway: evidence from the boundary between two macrocyclic units. Contributions to Mineralogy and Petrology 107, 403–414.

Nielsen, F.M., Campbell, I.H., McCulloch, M., Wilson, J.R., 1996. A strontium isotopic investigation of the Bjerkreim-Sokndal layered intrusion, southwest Norway. Journal of Petrology 37, 171–193.

Paludan, J., Hansen, U.B., Olesen, N.Ø., 1994. Structural evolution of the Precambrian Bjerkreim-Sokndal intrusion, south Norway. Norsk Geologisk Tidsskrift 74, 185–198.

Paterson, S.R., Vernon, R.H., Tobisch, O.T., 1989. A review of criteria for the identification of magmatic and tectonic foliation in granitoids. Journal of Structural Geology 11, 349–363.

Philpotts, A.R., 1967. Origin of certain iron–titanium oxide and apatite rocks. Economic Geology 62, 303–315.

Phinney, W.C., 1992. Partition coefficients for iron between plagioclase and basalt as a function of oxygen fugacity: implications for Archean and lunar anorthosites. Geochimica et Cosmochimica Acta 56, 1885–1895.

Robins, B., Tumyr, O., Tysseland, M., Garman, L.D., 1997. The Bjerkreim-Sokndal layered intrusion, Rogaland, SW Norway: evidence from marginal rocks for a jotunite parent magma. Lithos 39, 121–133.

Robinson, P., Kullerud, K., Tegner, C., Robins, B., McEnroe, S.A., 2003. Could the Tellnes ilmenite deposit have been produced by in-situ magma mixing? Norges Geologiske Undersøkelse Special Publication 9, 107–108.

Schärer, U., Wilmart, E., Duchesne, J.C., 1996. The short duration and anorogenic character of anorthosite magmatism: U–Pb dating of the Rogaland complex, Norway. Earth and Planetary Science Letters 139, 335–350.

Scoates, J.S., Chamberlain, K.R., 1997. Orogenic to post-orogenic origin for the 1.76 Ga Horse Creek anorthosite complex, Wyoming, USA. Journal of Geology 105, 331–343.

Tegner, C., 1997. Iron in plagioclase as a monitor of the differentiation of the Skaergaard intrusion. Contributions to Mineralogy and Petrology 128, 45–51.

Tegner, C., Wilson, J.R., Robins, B., 2005. Crustal assimilation in basalt and jotunite: constraints from layered intrusions. Lithos 83, 299–316.

Toplis, M.J., Carroll, M.R., 1995. An experimental study of the influence of oxygen fugacity on Fe–Ti oxide stability, phase relations, and mineral-melt equilibria in ferro-basaltic systems. Journal of Petrology 36, 1137–1170.

Vander Auwera, J., Longhi, J., 1994. Experimental study of a jotunite (hypersthene monzodiorite): constraints on the parent magma composition and crystallization conditions ($P$, $T$, $f_{O2}$) of the Bjerkreim-Sokndal layered intrusion (Norway). Contributions to Mineralogy and Petrology 118, 60–78.

Vander Auwera, J., Longhi, J., Duchesne, J.C., 1998. A liquid line of descent of the jotunite (hypersthene monzodiorite) suite. Journal of Petrology 39, 439–468.

Vander Auwera, J., Longhi, J., Duchesne, J.C., 2000. The effect of pressure on DSr (plag/melt) and DCr (opx/melt): implications for anorthosite petrogenesis. Earth and Planetary Science Letters 178, 303–314.

Vander Auwera, J., Weis, D., Duchesne, J.C., in press. Marginal mafic intrusions as indicators of downslope draining of dense residual liquids in anorthositic diapirs. Lithos.

van der Molen, I., Paterson, M.S., 1979. Experimental deformation of partially-melted granite. Contributions to Mineralogy and Petrology 70, 299–318.

Wilmart, E., Demaiffe, D., Duchesne, J.C., 1989. Geochemical constraints on the genesis of the Tellnes ilmenite deposit, southwest Norway. Economic Geology 84, 1047–1056.

Wilson, J.R., Overgaard, G., 2005. Relationship between the Layered Series and the overlying evolved rocks in the Bjerkreim-Sokndal intrusion, southern Norway. Lithos 83, 277–298.

Wilson, J.R., Robins, B., Nielsen, F.M., Duchesne, J.C., Vander Auwera, J., 1996. The Bjerkreim-Sokndal layered intrusion, southwest Norway. In: Cawthorn, R.G. (Ed.), Layered Intrusions. Elsevier, Amsterdam, pp. 231–255.